5-1966

A Preliminary Experimental Study of the Turbulence Decay in the Wake of a Hemisphere in Free-Surface Flow

Jiin-jen Lee
Utah State University

A PRELIMINARY EXPERIMENTAL STUDY OF THE TURBULENCE DECAY IN THE WAKE OF A HEMISPHERE IN FREE-SURFACE FLOW

by

Jiin-jen Lee

A report submitted in partial fulfillment
of the requirement for the degree

of

MASTER OF SCIENCE

in

Civil Engineering

Plan B

UTAH STATE UNIVERSITY
Logan, Utah

1966

ACKNOWLEDGMENTS

The writer wishes to express his deep appreciation to Dr. Gordon H. Flammer for his constant encouragement and invaluable advice on this study for the last two years. The opportunity to work under him as a research assistant through financial aid from the National Science Foundation was a most enjoyable experience to the writer.

The writer also expresses sincere gratitude to Dr. Gary Z. Watters for his careful review of the manuscript and his kindness in acting as the writer's major professor after Dr. Flammer left this country for Thailand.

Appreciation is also extended to Dr. Calvin G. Clyde and Dr. Cheng-lung Chen for their constructive comments and many hours of discussion in the course of the work. Through Dr. Clyde's instruction the writer's interest in the study of turbulence was inspired.

Special thanks are due to my wife, Sage, for her understanding, encouragement, and patience in typing the manuscript.

Jiin-jen Lee

TABLE OF CONTENTS

LIST OF FIGURES

CHAPTER I

INTRODUCTION

Flows observed in open channels are usually turbulent. The word "turbulent" describes a motion in which an irregular velocity fluctuation (mixing or eddying motion) is superimposed on the main stream motion. The essential characteristic of turbulent flow is that the turbulent fluctuations are random in nature.

If Reynold's rule of averaging is used, the Navier-Stokes equations for laminar flow may be transformed into the Reynold's equations, which hold true for turbulent mean motion. The solution of Reynold's equations will properly describe turbulent flow. Unfortunately, the number of unknowns exceeds the number of equations; therefore the use of the mathematical method to solve turbulent flow problems is extremely difficult and not possible at present.

The details of turbulent flow are so complicated that a statistical approach must be used. Extensive research has been done in this regard during the last few decades. G. I Taylor (1935) presented a statistical theory of turbulence based on the assumption of homogeneous isotropic turbulence. He introduced various concepts such as turbulence intensity, correlation coefficient, scale of turbulence, and energy spectrum. Kolmogoroff (1941) introduced the theory of locally isotropic

turbulence. He postulated that turbulent motion at large Reynold's number is locally isotropic whether or not the large scale motions are isotropic. He also introduced the concept that the small scale motions are mainly governed by viscous forces and the amounts of energy which are handed down to them from the large eddies. Other investigations of isotropic turbulence have been made by Karman (1938), Heisenberg (1948), Lin (1948), etc. Even for the simplest type of turbulence (i. e. isotropic turbulence), it is not possible to obtain the general solution to the equations because the details of turbulence are so complicated. Present knowledge about the statistical distribution of non-homogeneous turbulence is even less extensive. Therefore, before real use can be made of the statistical theory of turbulence much work must be done.

There is widespread interest in the structure and characteristics of turbulence in flowing water but the information available is still very limited and piecemeal. Considerable experimental research has been done on turbulence in air, using hot-wire anemometry. Because of the formidable difficulties of using the hot-wire in water, very few studies have been done in water flow. This preliminary experimental study is to observe the turbulence decay behind a hemisphere in a free surface flow, in which the size of hemisphere is of the same order of magnitude as the depth of flow and the free turbulence (from the wake of the hemisphere) is as important as the wall turbulence (from the presence of the channel bed).

CHAPTER II

BRIEF SUMMARY OF THE STATISTICAL THEORY OF TURBULENCE

Equations Governing Turbulent Flow

In the derivation of the equations of turbulent flow, it is generally assumed that the motion can be separated into a mean flow, whose velocity components are $\overline{U}_1$, $\overline{U}_2$, $\overline{U}_3$, and a superposed turbulent velocity fluctuation whose components are u_1, u_2, u_3, the mean values of which are zero.

The Reynold's rule of averaging states that if A and B are dependent variables which are being averaged and S is any one of the space variables x, y, z or the time t, then $\overline{\frac{\partial A}{\partial S}} = \frac{\partial \overline{A}}{\partial S}$ and $\overline{\overline{A} \cdot B} = \overline{A} \cdot \overline{B}$ where the bar denotes a mean value. The time average is defined as

$$\overline{A}\,(x, y, z, t) = \frac{1}{T} \int_{t-\frac{T}{2}}^{t+\frac{T}{2}} A\,(x, y, z, \tau)\, d\tau \quad . \quad . \quad . \quad . \quad (1)$$

which is independent of the time t . When the mean flow is not varying, the time average is the natural mean value to use. Besides the time average, there is the space average (as in the case for finding the average velocity for velocity gradient flow) and the statistical average (ensemble average) which is the average taken over the infinite number of identical systems. The statistical average, which should be used if a rigorous general statistical theory is to be introduced, is

not attainable for experimental studies. Most of the averages are consequently based on the time average.

The equation of continuity of an incompressible fluid when averaged becomes

$$\frac{\partial \bar{U}_i}{\partial x_i} = 0 \qquad i = 1, 2, 3 \quad . \quad . \quad . \quad . \quad . \quad . \quad . \qquad (2)$$

The Navier-Stokes equations are

$$\rho \frac{\partial V_i}{\partial t} = \frac{\partial}{\partial x_j} (\sigma_{ij} - \rho V_i V_j) \quad . \quad . \quad . \quad . \quad . \quad . \quad . \qquad (3)$$

where $V_i = \bar{U}_i + u_i \qquad i = 1, 2, 3$

$$j = 1, 2, 3$$

and σ_{ij} is the stress tensor due to pressure and viscous forces.

If the mean value is taken from equation (3) then, according to the Reynold's rule of average,

$$\rho \frac{\partial \bar{U}_i}{\partial t} = \frac{\partial}{\partial x_j} (\bar{\sigma}_{ij} - \rho \bar{U}_i \bar{U}_j - \rho \overline{u_i u_j}) \quad . \quad . \quad . \qquad (4)$$

If equations 3 and 4 are compared, it is seen that they are the same except that in equation (4) there is an additional term called the Reynold stress (τ_{ij}),

$$\tau_{ij} = -\rho \overline{u_i u_j}$$

which represents the mean rate of momentum transfer across a surface due to the velocity fluctuations. When the mean flow is not varying, then the time average is taken at every point, and the physical interpretation of the Reynold's stress is clear. But if the space average is taken, then the interpretation of the Reynold's stress as a local stress is not as direct. When the statistical average is used the physical interpretation of an average quantity as an apparent stress is even more difficult, since the average momentum transfer is not directly associated with any one particular system. Thus if the general theory is developed on the basis of statistical averages, an ergodic theorem must be developed to connect the time average and the statistical average. Unfortunately there is not such a theorem available at present.

Turbulent Intensity

In applied statistics, "variance" (mean square) and "standard deviation" (a positive square root of the variance, sometimes called Root-Mean-Square) are commonly used for measure of the spread of the probability distribution curve, or in other words, a measure of the deviation from the mean value. By the basic definition of variance in statistics, it is a "second moment about the mean of the distribution of a random variable" namely,

$$\mu_2 = E\left[(x-\mu_1)^2\right] = \int_{-\infty}^{\infty} (x-\mu_1)^2 f(x)\, dx$$

where μ_2 represents the variance, μ_1 represents the mean, x is a random variable, and $f(x)$ is the distribution function of the random variable. The positive square root of the variance of the fluctuating velocity corresponds to turbulent intensity. Since it has already been pointed out that the statistical average is experimentally impossible, the turbulent intensity is usually defined in a time average sense. So the intensity of turbulence is written as

$$u' = \left[\frac{\sum_{i=1}^{n} (V_i - \bar{U}_i)^2}{n}\right]^{\frac{1}{2}} = \sqrt{\overline{u^2}}$$

$$= \left[\frac{1}{\Delta t}\int_0^{\Delta t} (V - \bar{U})^2\, dt\right]^{\frac{1}{2}}$$

Because it is sometimes more useful to formulate a dimensionless term, the relative intensity of turbulence is defined as

$$R.I. = \frac{\sqrt{\overline{u_i^2}}}{\bar{U}_i} = \frac{u_i'}{\bar{U}_i} \qquad i = 1, 2, 3$$

By the intensity one will be able to describe how strong the fluctuation is about the mean value; however, the intensity refers only to the magnitude, not the frequency, of fluctuations.

Correlation Tensor

Since a basic theoretical treatment of the frequency distribution function has not yet been developed to an applicable stage, current statistical theories of turbulence are usually concerned with readily measurable quantities. This practice has the advantage that experimental information can be easily resorted to when purely theoretical considerations become uncertain. Instead of dealing with the distribution function, the correlation function, which can be more readily measured by hot-wire technique, is used.

The study of correlation was first initiated by G. I. Taylor in 1935. The importance of the correlation methods is heightened by the fact that many correlation coefficients are measurable, so that any theoretical forecasts made about them can be checked by experiment. In his theory, Taylor makes much use of the correlation between the components of the velocity fluctuations at neighboring points. The components of the fluctuating velocity at one point A are denoted by u_1, u_2, u_3, and at another point A' by u'_1, u'_2, u'_3, the correlation coefficient between any of the u_i and u'_j where i, j = 1, 2, 3 is defined as

$$R_{ij} = \frac{\overline{u_i \cdot u'_j}}{\sqrt{\overline{u_i^2}}\ \sqrt{\overline{u'^2_j}}}$$

Von Karman (1948) pointed out that R_{ij} forms a tensor of the second order.

Correlation is not restricted to the above mentioned double-velocity correlation; instead there are triple-velocity correlations (which form a tensor of order three), and the correlations involving pressure and velocity fluctuation.

It is interesting to point out that the correlation between longitudinal and lateral components of velocity fluctuation at a single point is a very important parameter since these correlation coefficients are directly related to the Reynold's stress or eddy stresses. By definition, the correlation between the u_1 and u_2 components of velocity fluctuation is:

$$R_{u_1 u_2} = \frac{\overline{u_1 \cdot u_2}}{\sqrt{\overline{u_1^2}}\ \sqrt{\overline{u_2^2}}}$$

In this equation since $R_{u_1 u_2}$ is measurable with the correlator and $\sqrt{\overline{u_1^2}}\ \sqrt{\overline{u_2^2}}$ are measurable with an RMS meter; thus the term $\overline{u_1 u_2}$, which is a part of the Reynold's stress, can be calculated.

Another kind of correlation is obtained by delaying the signal from a point. This "autocorrelation coefficient" correlates the signal at the same point but at different times t and $t + \tau$ and is expressed as:

$$R_i(\tau) = \frac{u_i(t)\ u_i(t+\tau)}{\overline{u_i^2}}$$

From the auto-correlation curve at least four pieces of information can be obtained. First, the microscale of turbulence; second, the macroscale of turbulence; third, the rapidity with which the relatedness is lost with time delay; and fourth, the periodicity which the fluctuation signal possesses.

Scale of Turbulence

It was pointed out earlier that turbulent flows contain various sizes of eddies. A search was initiated for a means of representing the size of the eddies in the flowing stream. Motivated by this, Taylor (1935) introduced a number of scales which characterize various statistical aspects of turbulence, i. e., microscale and macroscale of turbulence. It may be postulated that the local change of the turbulent fluctuation is caused by the smallest eddies present in the turbulent flow field. The microscale of turbulence is then considered to be a measure of the average dimension of the smallest eddies. It is also stated in Kolmogoroff's hypothesis (1941) that the smallest eddies are mainly responsible for the turbulent energy dissipation. The microscale of turbulence is, therefore, sometimes called dissipation scale or dissipation length.

Detailed discussion of the definition of the scale of turbulence can be found in "Turbulence" by Hinze (1959) . The microscale of turbulence is a measure of the curvature of the longitudinal correlation

function at its origin. Unfortunately the shape of the correlation curve at its vertex is not usually accurately known, since an accurate measurement of the correlation is not simple when the correlation coefficient is close to unity, therefore, the microscale based on the correlation curve is not very practical.

Townsend (1947) suggested a simpler method for measuring the microscale λ_f which can be accomplished with the random signal indicator and correlator. The equation is:

$$\lambda_f = \overline{U} \cdot \frac{\sqrt{\overline{u^2}}}{\sqrt{\overline{\left(\frac{du}{dt}\right)^2}}}$$

where $\overline{U}$ is the mean flow velocity, and

u is the turbulent fluctuation .

The macroscale of turbulence L_{x_i} is defined as

$$L_{x_i} = \int_0^\infty R(x_i)\, dx_i , \quad i = 1, 2, 3 .$$

From the afore mentioned definition, the macroscale of turbulence is obtained by integrating the correlation curve. The macroscale is a measure of the size of the (low-frequency eddies of the turbulent field which contain most of the turbulent energy.

Another macroscale using the autocorrelation curve may be defined as

$$L\tau_i = \bar{U}_i \int_0^\infty R_i(\tau)\, d\tau$$

which has the dimensions of length.

CHAPTER III

INSTRUMENTATION AND METHOD OF PROCEDURE

Description of Apparatus

Flume

The measurements of this study were performed in a 3-foot wide, 2-foot deep and 24-feet long tilting flume, located in the Utah Water Research Laboratory (as shown in Figure 1). The slope of the flume is adjustable from 0 to 4 per cent. The inlet pipe supplied the water through the bottom of the head tank. The water was distributed smoothly by the newly introduced diffusion partition. At the entrance of the flume, a sluice gate was provided for regulating the flow velocity. A hemisphere of 5 inches diameter was located in a position 14 feet downstream from the sluice gate. All tests for this experiment were performed as open-channel flow past a stationary hemisphere.

Heat-flux system constant-temperature anemometer (model 1010)

Dual channels of the Heat-flux system hot-wire anemometer manufactured by Thermo-Systems, Inc. were used for this study (Figures 2, 3, and 4 show the instrumentation set-up) . The anemometer provided a constant temperature compensation for hot-wires, hot-films and other sensors. The idea behind the constant-temperature system is to minimize the effect of the thermal inertia of the probe by keeping

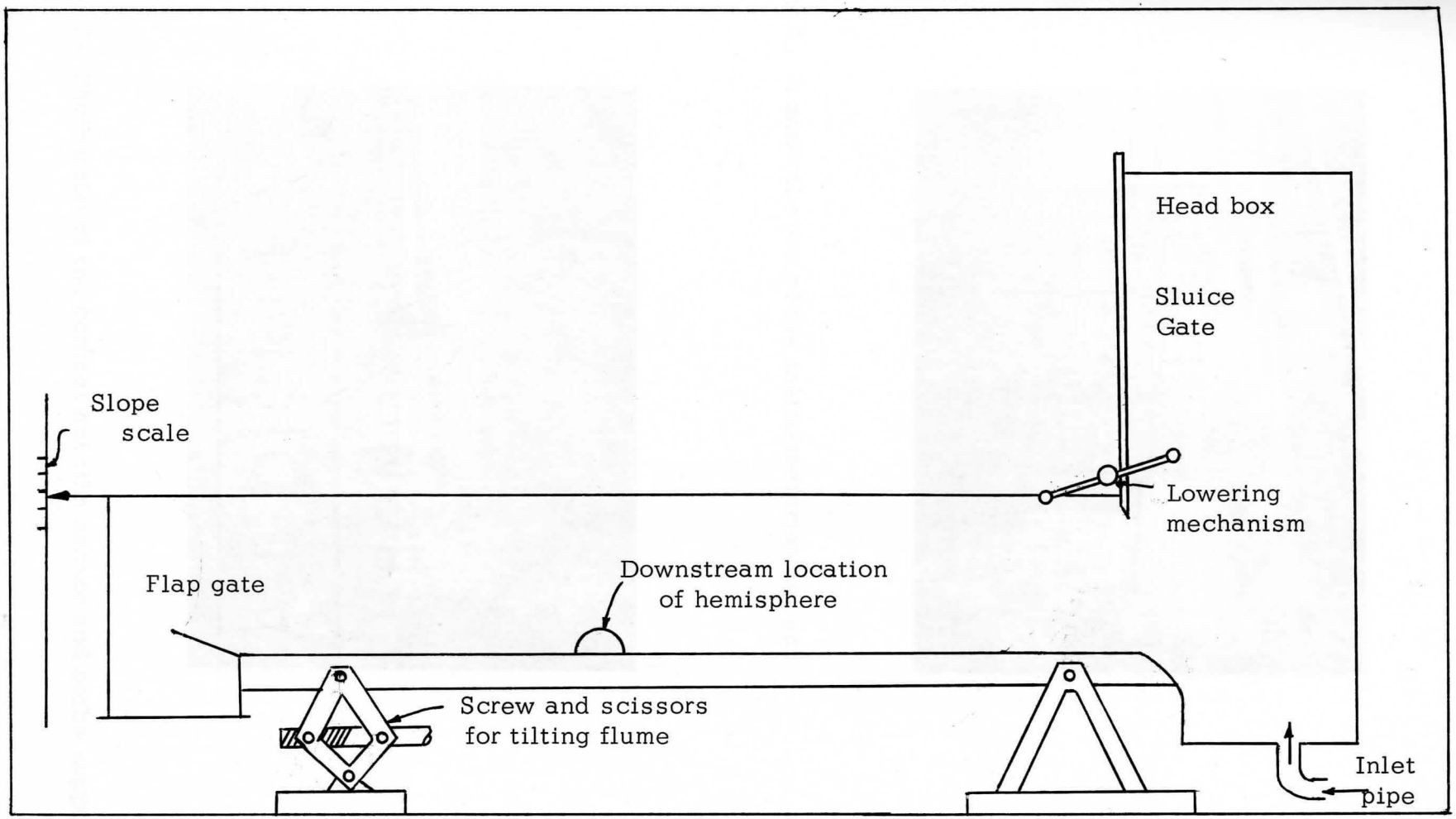

Figure 1. Schematic of the 3 foot wide by 2 foot deep by 24 foot long tilting flume used for testing.

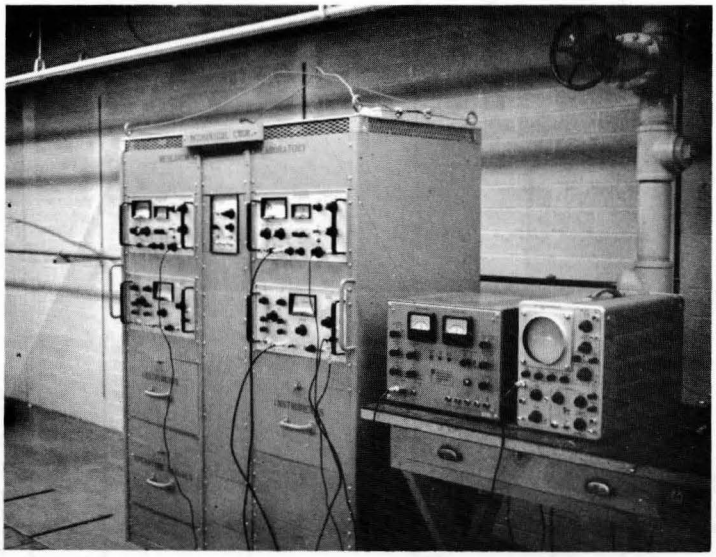

Figure 2. A general view of the instrumentation set up.

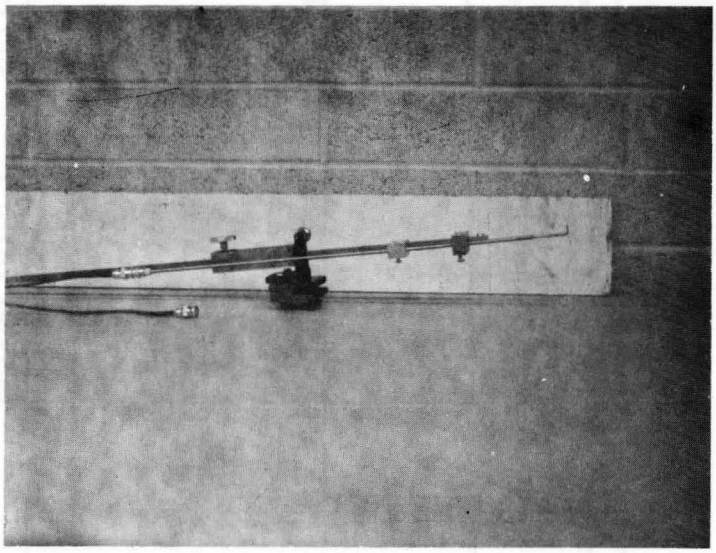

Figure 3. Photograph of the conical hot film sensor and probe support.

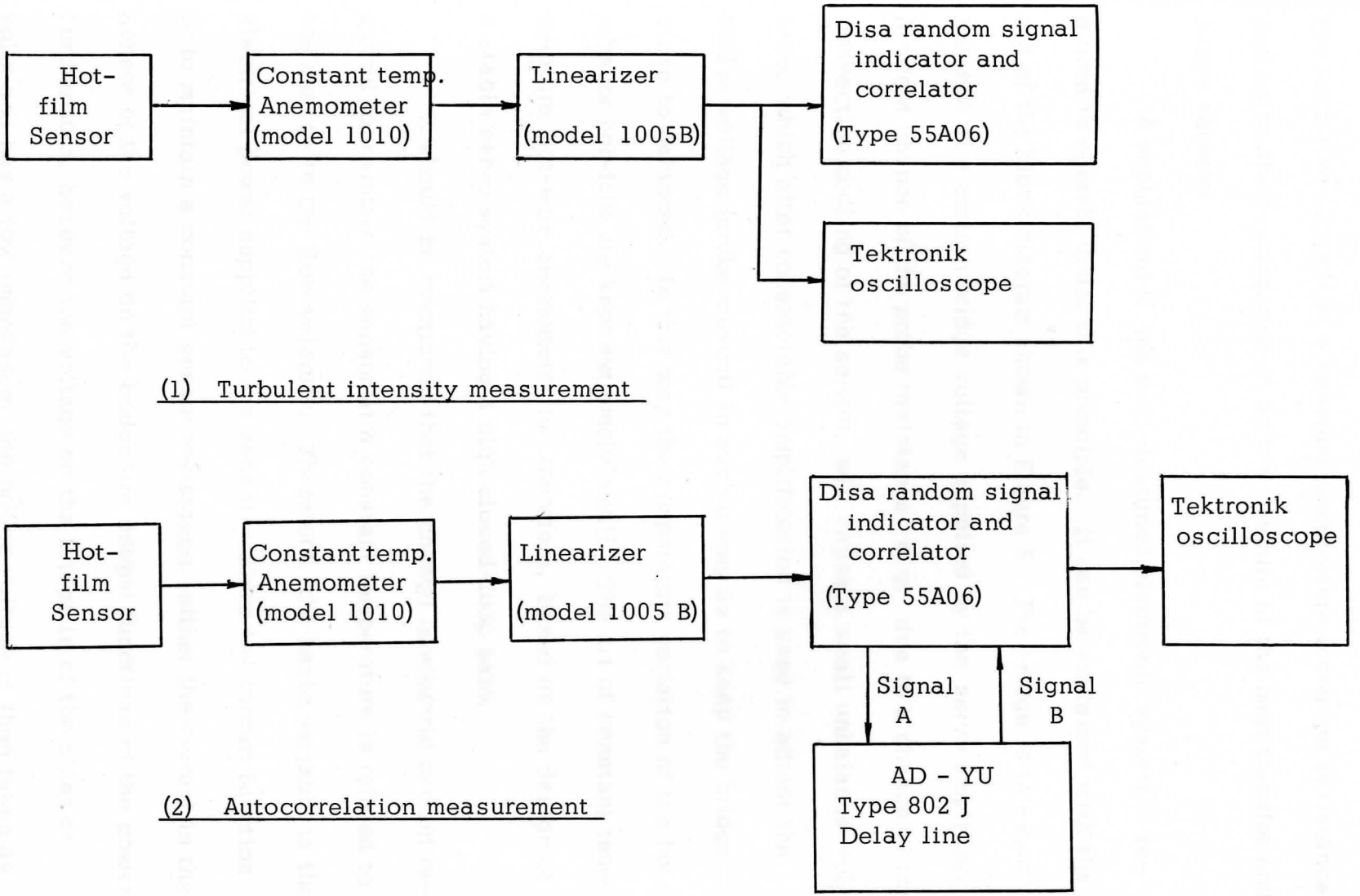

Figure 4. Block diagram of the instrumentation system.

the sensitive element at a constant temperature (constant resistance) and using the heating current as the measure of the heat transfer and hence velocity.

A sophisticated and well-designed electronic system is required to operate under this principle. It can be explained with the aid of the block diagram shown in Figure 5. The bridge is in exact balance at a certain bridge voltage supplied by the servo amplifier. A slight change of the probe resistance, e. g. due to a change of the convective cooling of the sensor, will cause a small unbalance voltage, which after considerable amplification is used to adjust the bridge voltage (probe current) in such a way as to keep the bridge close to balanced. In this way the temperature variation of the hot-wire or hot-film are kept extremely small. The art of constant temperature hot-wire anemometry is, therefore, based on the design of a stable servo system having a high closed-loop gain.

It should be mentioned that the change in electric current required to maintain the sensor at a constant temperature is related to the change in the flow velocity. Therefore, the basic variable is the electrical power supplied to the sensor. Since the circuit function is to maintain a constant sensor resistance, either the current in the sensor or the voltage on the bridge are unique functions of the power. Furthermore, because the voltage on the bridge is of the order of volts and has a low impedance, the bridge voltage is then taken as

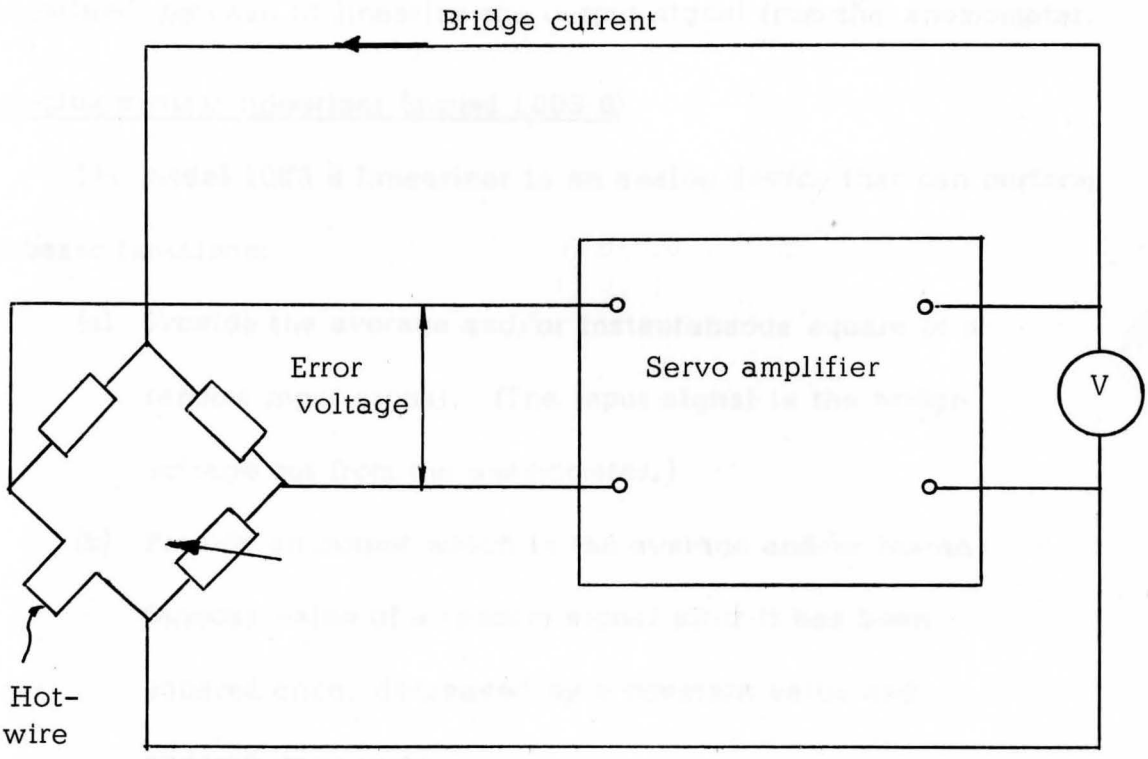

Figure 5. Constant-temperature anemometer, principle of operation.

an output of the anemometer. Unfortunately, the bridge voltage is not a linear function of the velocity, instead, it varies approximately as the one-fourth power of the velocity. In order to get a proper picture of the velocity fluctuations it is recommended that the "Linearizer" be used to linearize the output signal from the anemometer.

Heat-flux system linearizer (model 1005 B)

The model 1005 B Linearizer is an analog device that can perform two basic functions:

(a) Provide the average and/or instantaneous square of a random input signal. (The input signal is the bridge voltage out from the anemometer.)

(b) Provide an output which is the average and/or instantaneous value of a random signal after it has been squared once, decreased by a constant value and squared once more.

The first squaring process of the aforementioned basic function is used when the electrical power input to the sensor from the circuit is desired. The second squaring process is used when the flow velocity is desired. Since in this study the velocity is the main item of interest, the second squaring process is used in order to obtain a linear relationship between the output of the linearizer and the flow velocity.

Hot-film sensor

Two kinds of sensors, quartz-coated cylindrical hot-film and

quartz-coated conical hot-film, have been used in this study. Figure 6 shows the configuration of these two sensors. Only the conical hot-film sensor proved successful.

Because the flowing water is taken directly from the Logan First Dam, the impurities in water such as sediment and algae, etc. were deposited on the film sensor. This deposition of impurities changed the signal continually, until the sensor had to be cleaned completely. The fact that this change of calibration of the sensor occurred over a short period made the measurement impossible. The conical sensor proved much better in this respect. Because of its shape the impurities were not so easily deposited.

The sensor is mounted to the probe (sensor holder) and connected to the probe support which was connected to the probe terminal in the anemometer by a fifteen-foot special co-axial cable.

DISA random-signal indicator and correlator (model 55A06)

The DISA random-signal indicator is designed for measuring the root-mean-square voltage of the two electrical inputs as well as the correlation number relating the two signals. Two meters indicate the true root-mean-square voltage and the correlation coefficient regardless of wave form. The RMS voltmeter can be used to measure the RMS of the signal A, B, A + B, A - B, $\tau \frac{dA}{dt}$. Therefore the unit also serves the purpose of obtaining sum and difference measurements of two random signals. The ratiometer is designed for measuring the

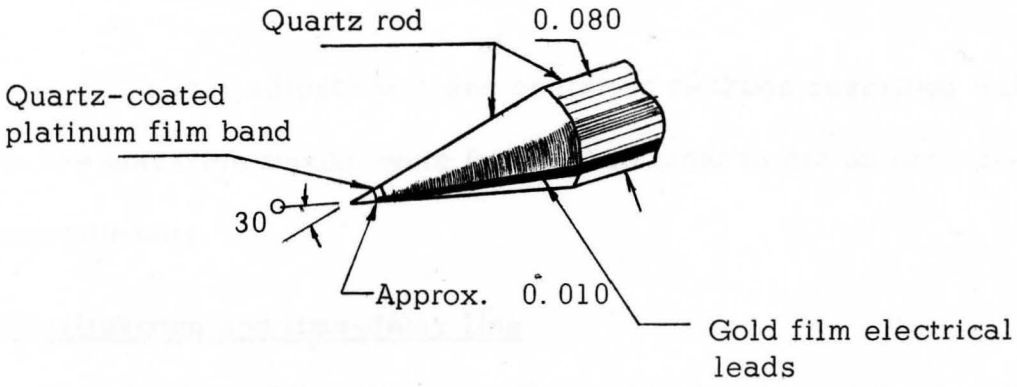

(1) Conical hot-film

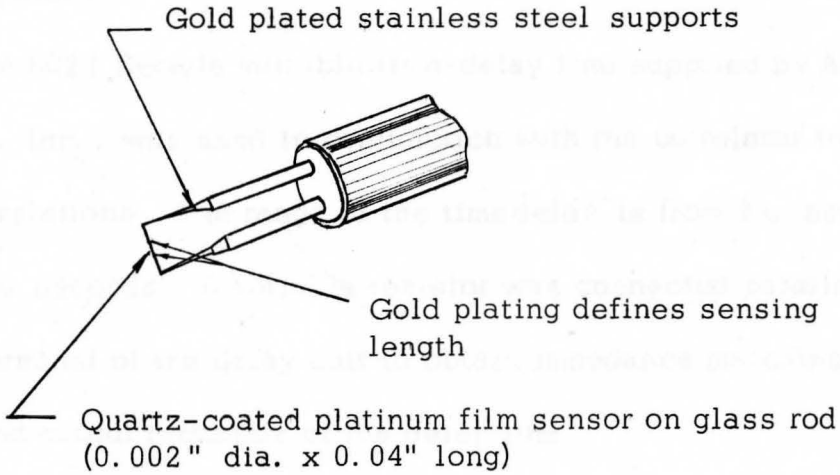

(2) Cylindrical hot-film

Figure 6. Configuration of the cylindrical hot-film and conical hot-film sensor.

root-mean-square value of the following ratios:

$$\frac{A}{B}, \quad \frac{A+B}{A-B}, \quad \frac{A}{\tau \frac{dA}{dt}}.$$

Various adjustments and operation methods described fully in the operation manual were followed in order to get an accurate measurement.

Oscilloscope and time-delay line

A tektronik oscilloscope (Type 515 A) was used to view the output signal from the anemometer, linearizer, or random-signal indicator and correlator. Because the recorded measurement was not made on the oscilloscope, a calibration of the oscilloscope was not required.

Type 802 J Decade variable time-delay line supplied by AD-YU Electronics, Inc., was used in conjunction with the correlator to obtain the autocorrelations. The range of the time delay is from 2 μ seconds to 200,000 μ seconds. A variable resistor was connected parallel to the input terminal of the delay unit to obtain impedance matching at the input and output terminals of the delay line.

Method of Procedure

Measurement of the mean velocity by means of the Anemometer and Linearizer (calibration of the Linearizer by pitot tube)

The following procedure of calibration was used:

(a) The sensor exposed to the flowing water was connected to the PROBE terminal in the anemometer.

(b) The cold resistance was measured when the unit was in STAND-BY position.

(c) The probe was heated by a prescribed over-heat ratio (over-heat ratios from 1.05 to 1.10 have been tried). This probe resistance (hence temperature) will be kept constant automatically by the anemometer.

(d) The sensor was energized by setting some stand-by voltage (5 volts to 10 volts have been tried) .

(e) The anemometer was then set to the RUN position.

(f) The bridge output of the anemometer was connected to the INPUT jack of the "Linearizer."

(g) The GAIN ADJUST and ZERO ADJUST for both squaring circuits were adjusted to zero the meter.

(h) The power for zero velocity was measured by exposing the probe to still water with the same temperature as the flowing water.

(i) The meter of item (h) was then zeroed, (at this time the function switch was in SQUARING CIRCUIT I position).

(j) The function switch was set to SQUARING CIRCUIT 2 position; the meter reading is then a linear function of the velocity.

(k) The pitot tube for measuring the mean velocity was set in position at exactly the same point as the hot-film probe was located. The velocity head was read and converted to the true velocity in feet per second.

(l) Different velocities were then measured in order to get a calibration curve between the linearizer output and the true mean velocity (as shown in Figure 7) .

Measurement of the relative intensity

(a) The flow is regulated to meet the prescribed water depth and the mean velocity. (The velocity at the point 0. 6 depth from the bottom proved to be very close to the mean velocity.)

(b) The signal was linearized as described in section (l) and the output signal of the linearizer was connected to the input "A" of the random-signal indicator and correlator.

(c) The undisturbed velocity profile was measured. The mean velocity was obtained from linearizer, the RMS value was obtained from the RMS meter. The undisturbed velocity profile is defined as the velocity profile without the hemisphere, measured at the position to be occupied by the center of the hemisphere.

(d) The hemisphere was attached to the bottom of the flume.

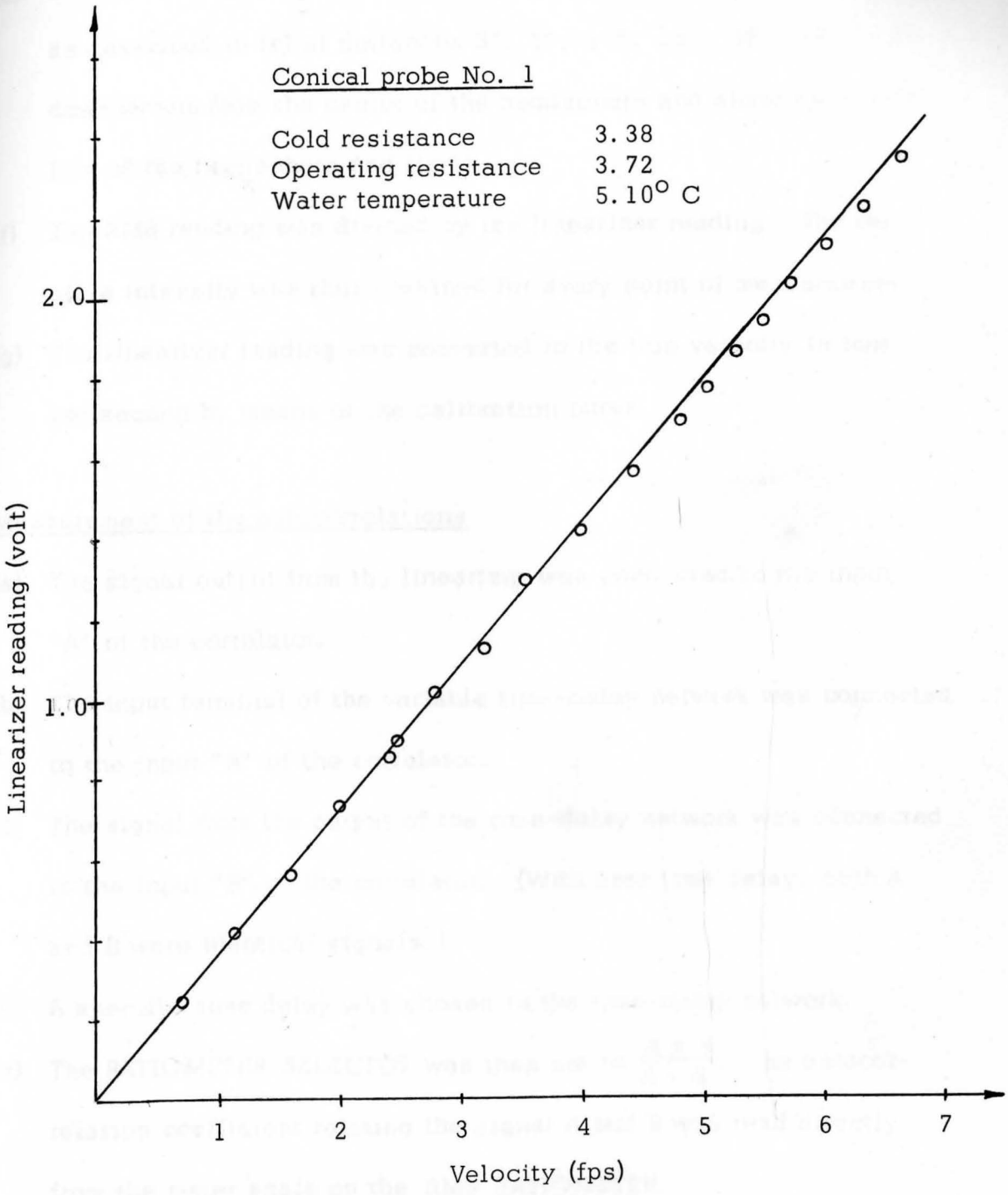

Figure 7. A typical example of the calibration curve.

(e) The probe carriage was moved into position to measure the profiles as described in (c) at distances 3", 5", 10", 15", 20", 30", etc. downstream from the center of the hemisphere and along the center line of the hemisphere and flume.

(f) The RMS reading was divided by the linearizer reading. The relative intensity was thus obtained for every point of measurement.

(g) The linearizer reading was converted to the true velocity in feet per second by means of the calibration curve.

Measurement of the autocorrelations

(a) The signal output from the linearizer was connected to the input "A" of the correlator.

(b) The input terminal of the variable time-delay network was connected to the input "A" of the correlator.

(c) The signal from the output of the time-delay network was connected to the input "B" of the correlator. (With zero time delay, both A and B were identical signals.)

(d) A specific time delay was chosen in the time-delay network.

(e) The RATIOMETER SELECTOR was then set to $\frac{A + B}{A - B}$, the autocorrelation coefficient relating the signal A and B was read directly from the meter scale on the RMS RATIOMETER.

(f) The same procedure was repeated for increasing time delay. Thus the autocorrelation curve, showing the autocorrelation coefficient

vs. the time delay, was then obtained.

At zero time delay, the value of the correlation coefficient was found to be nearly one as it should be.

CHAPTER IV

ANALYSIS OF RESULTS AND DISCUSSION

Autocorrelation in the Wake of the Hemisphere

The autocorrelation measurements were performed in one flow condition S5-250-3 (S5 signifies a 5-inch hemisphere, 250 indicates that the undisturbed water depth is 0.25 feet, 3 shows run number 3 which corresponds to a Froude number of 2.5) . The Froude number always refers to the undistrubed flow condition. The measurements were taken at points 3", 5", 10", 20", and 30" behind the center of the hemisphere and along the center line of the flume (also the center line of the hemisphere) and the results are shown in Figures 8 through 13. The point of measurement was at a point $x_2 = 0.15$ feet above the channel bed (relative depth $x_2/k = 0.75$). Several different relative depths such as $x_2/k = 0.50, 0.60, 0.80, 0.85$ were tried. Best correlation was found at a value of $x_2/k = 0.75$.

From the autocorrelation curves shown in Figures 8 through 13, several inferences can be made:

(1) The periodicity of the signal is clearly shown in Figure 8; the period is about 6 milliseconds. This strong periodic phenomena is similar to the so called Karman vortex street, which is known to appear in the wake of a sphere or a cylinder in an infinite flow field for Reynold's numbers

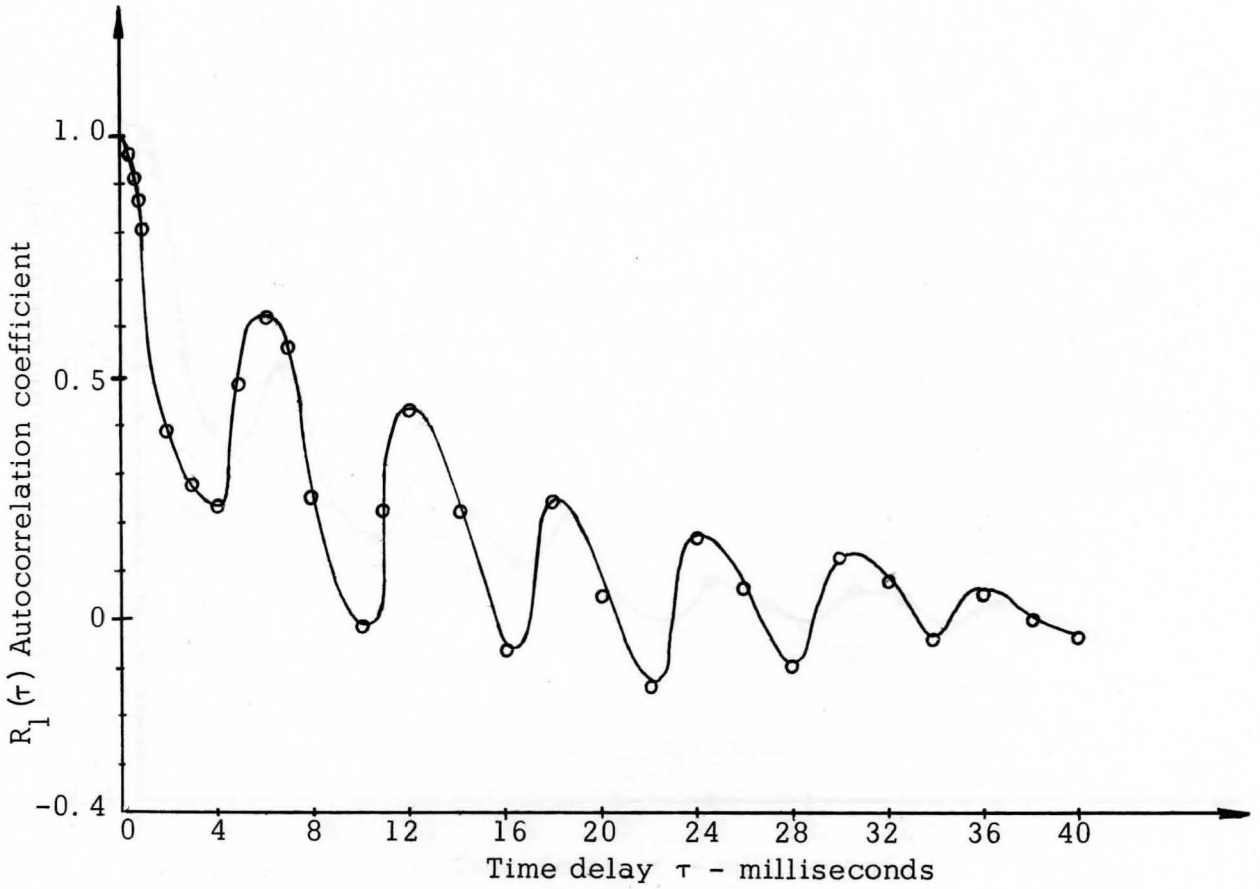

Figure 8. Autocorrelation curve for 3" behind the hemisphere at the depth of 0.15 feet from the bed. (Undisturbed flow: F_r = 2.5, depth 0.25 ft.)

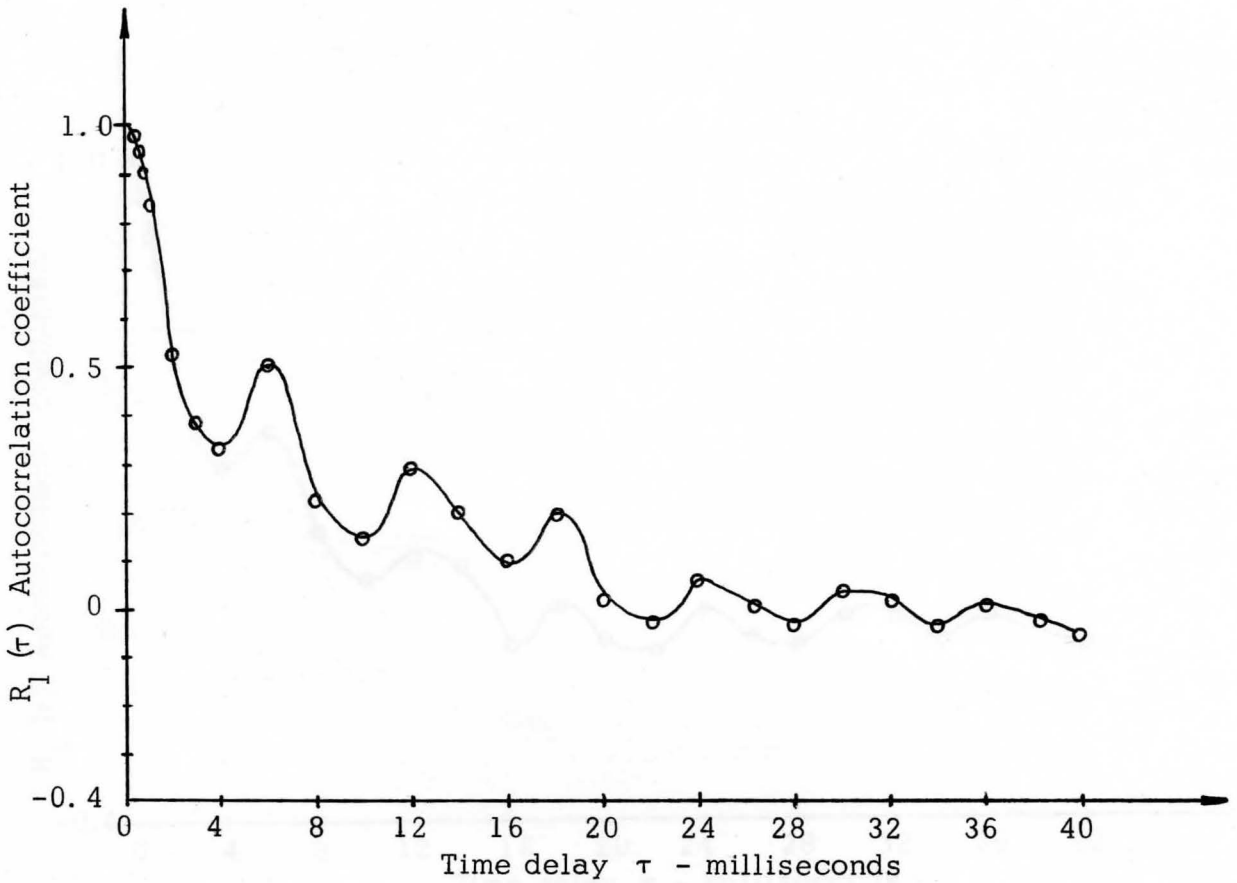

Figure 9. Autocorrelation curve for 5" behind the hemisphere at the depth of 0.15 feet from the bed. (Undisturbed flow: F_r = 2.5, depth 0.25 ft.)

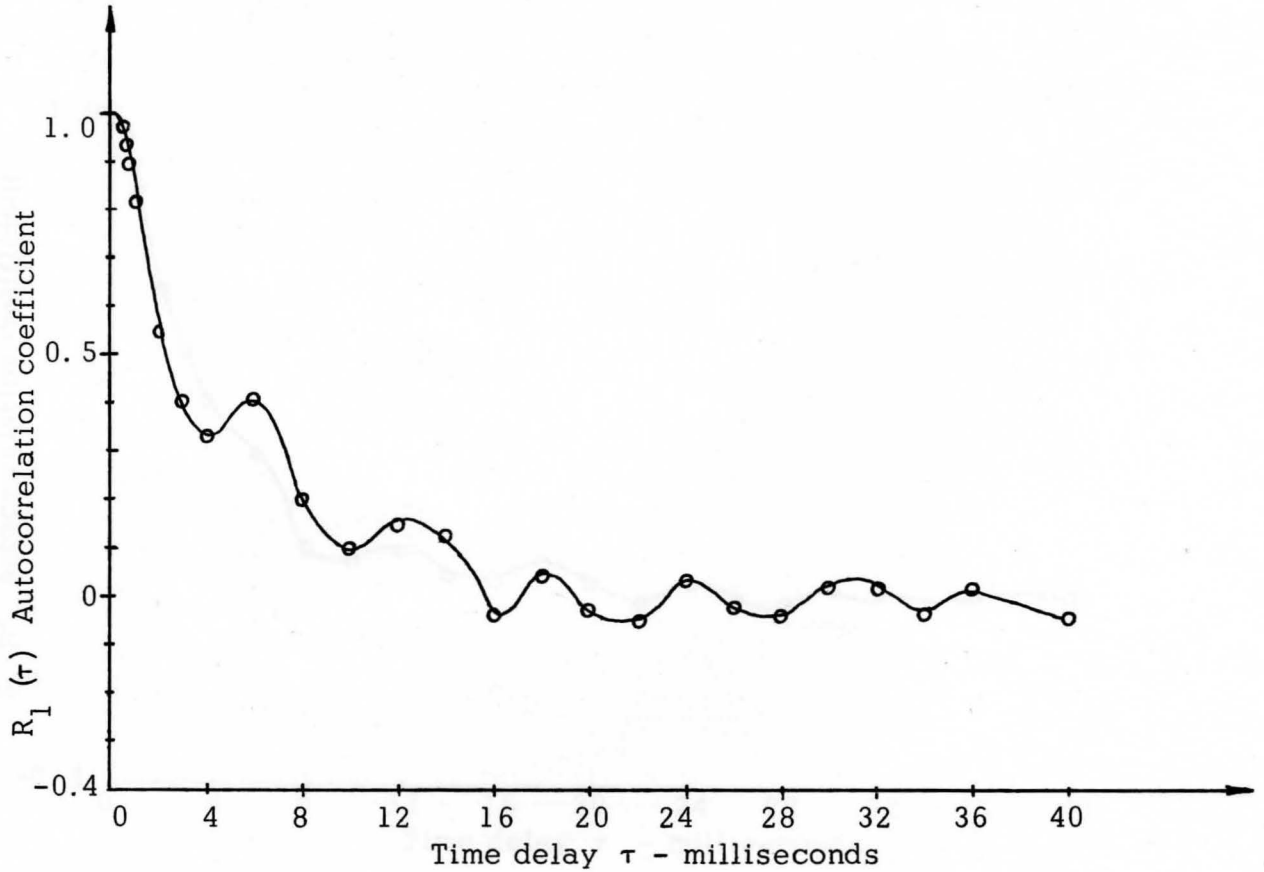

Figure 10. Autocorrelation curve for 10" behind the hemisphere at the depth of 0.15 feet from the bed. (Undisturbed flow: F_r= 2.5, depth 0.25 ft.)

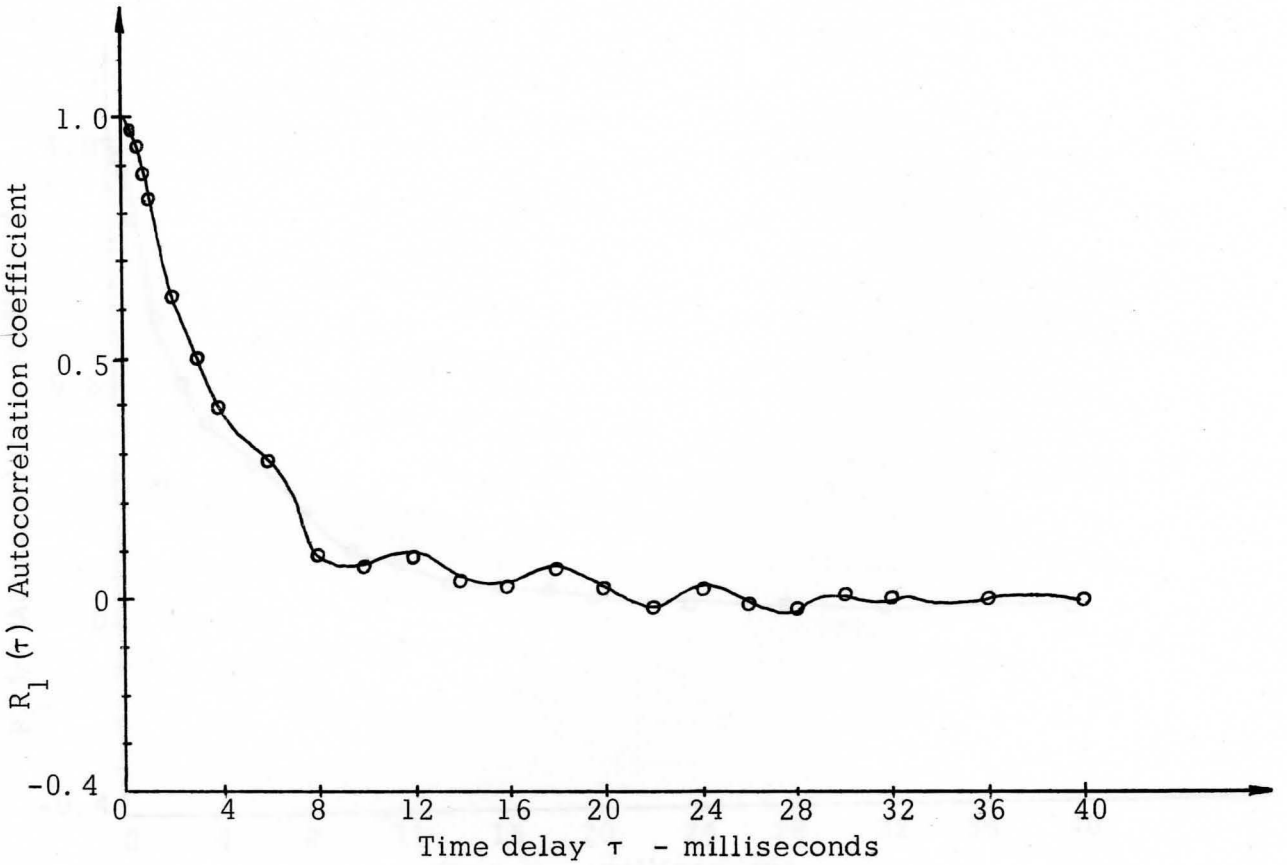

Figure 11. Autocorrelation curve for 15" behind the hemisphere at the depth of 0.15 feet from the bed. (Undisturbed flow: $F_r = 2.5$, depth 0.25 ft.)

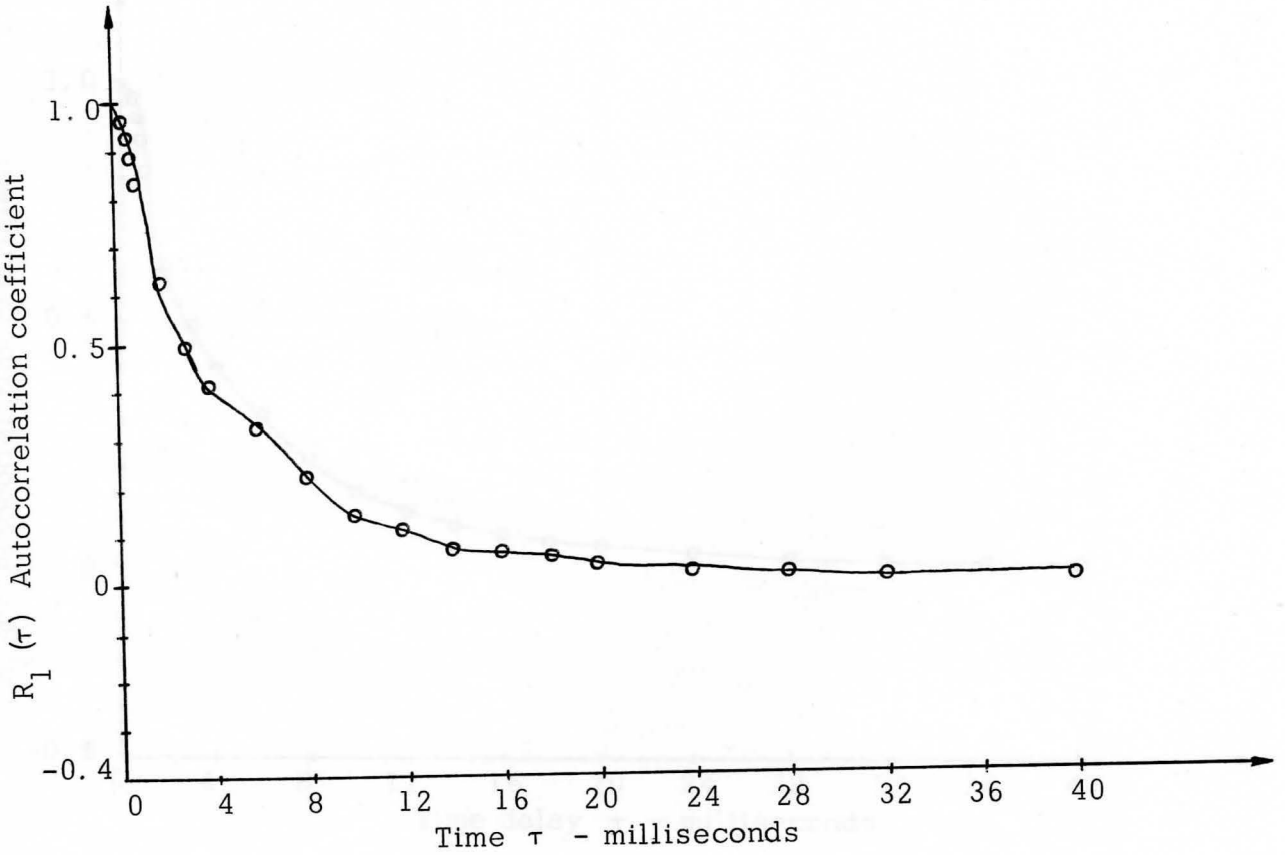

Figure 12. Autocorrelation curve for 20" behind the hemisphere at the depth of 0.15 feet from the bed. (Undisturbed flow: F_r = 2.5, depth 0.25 ft.)

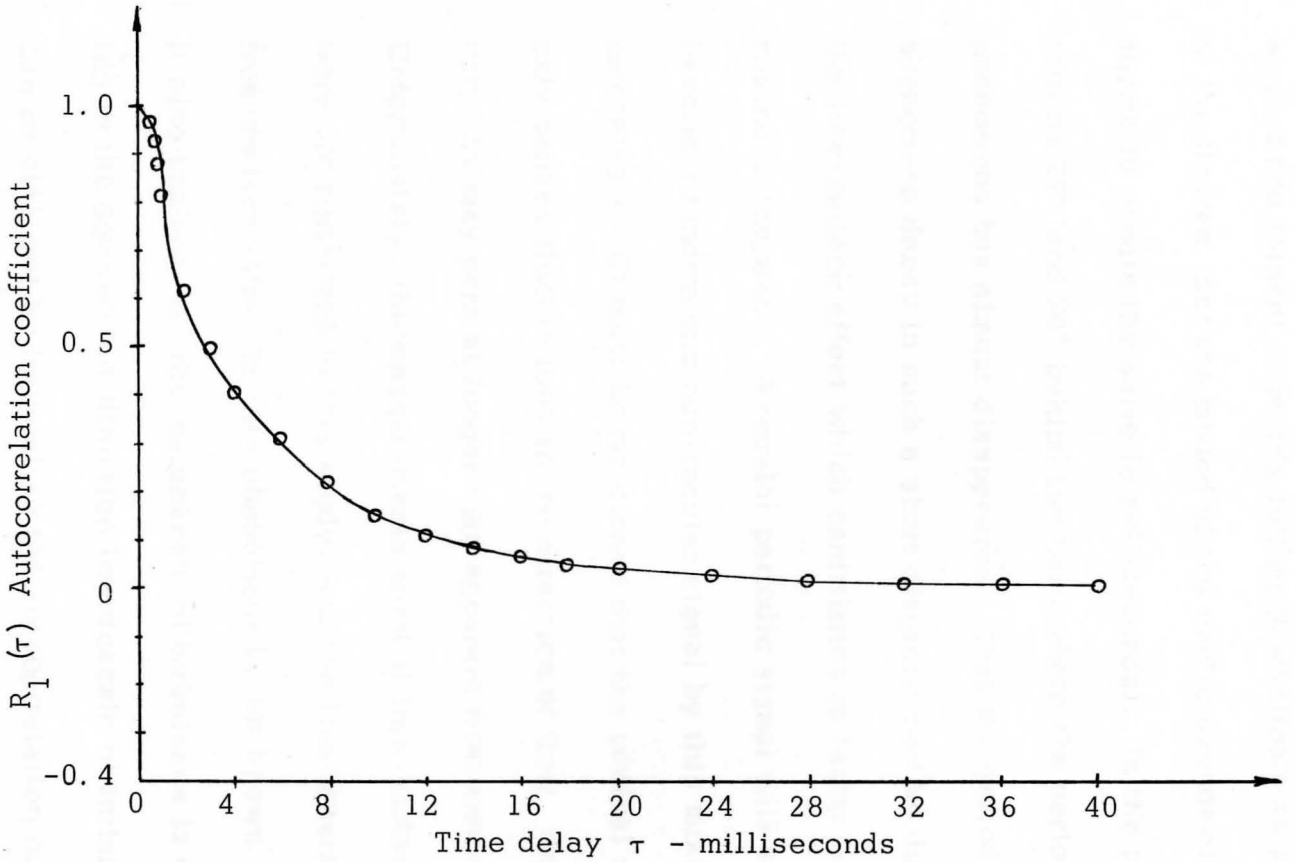

Figure 13. Autocorrelation curve for 30" behind the hemisphere at the depth of 0.15 feet from the bed. (Undisturbed flow: $F_r = 2.5$, depth 0.25 ft.)

between 10^3 and 10^5.

(2) The fluctuation in the autocorrelation curve becomes weaker and weaker at points further downstream as shown in the figures, but the period of the cyclic phenomena seems to remain the same (6 milliseconds). In the positions 20" and 30" behind the hemisphere the periodic phenomena has almost disappeared. That the periodic phenomena decay in such a short distance may be due to the free-surface effect which contributes to faster irregular mixing in the wake. A regular periodic signal will soon become a random and non-regular signal by this mixing mechanism. (It must be mentioned that the conical sensor only senses fluctuations in the direction of flow, thus the vorticity may persist longer than apparent from measurements.) Unfortunately, the measurements without free-surface effects were not performed in this study, and the true extent of the free-surface effect on this phenomena is not known.

(3) It also implied that the macroscale of turbulence is decreasing in the downstream direction (macroscale of turbulence can be obtained by integrating the autocorrelation curve). This agrees with the general decay process in which the bigger eddies break down to smaller eddies.

If the transverse space correlation could be measured, the periodicity in the transverse direction could probably be discovered and then the region of the vorticity could be deduced. Unfortunately, this could not be done for this report, because only one probe support was available. Space correlation is not possible without two probes.

Relative Intensity in the Wake of the Hemisphere

Undisturbed velocity profile

Six flow conditions with two different depths, 0.208 feet and 0.25 feet at 3 different Froude numbers: 1.5, 2.0, and 2.5, have been tested. The undisturbed velocity profile—the velocity profile before the hemisphere was introduced—was measured before any turbulence measurements were made in the wake region. The turbulent intensity for the undisturbed velocity profiles for 3 flow conditions at a depth of 0.25 feet are shown in Figure 14.

The results agree with the results published by Rao (1965) except in the region close to the water surface. Since the friction in the channel bed produces the so called "wall turbulence," the region close to the channel bed showed a higher relative intensity. As the point of measurement moved further above the channel bed, the wall turbulence effect became less and less. But in the region close to the water surface, the relative intensity showed an increase again. This fact may result from the free-surface roughness producing additional turbulence.

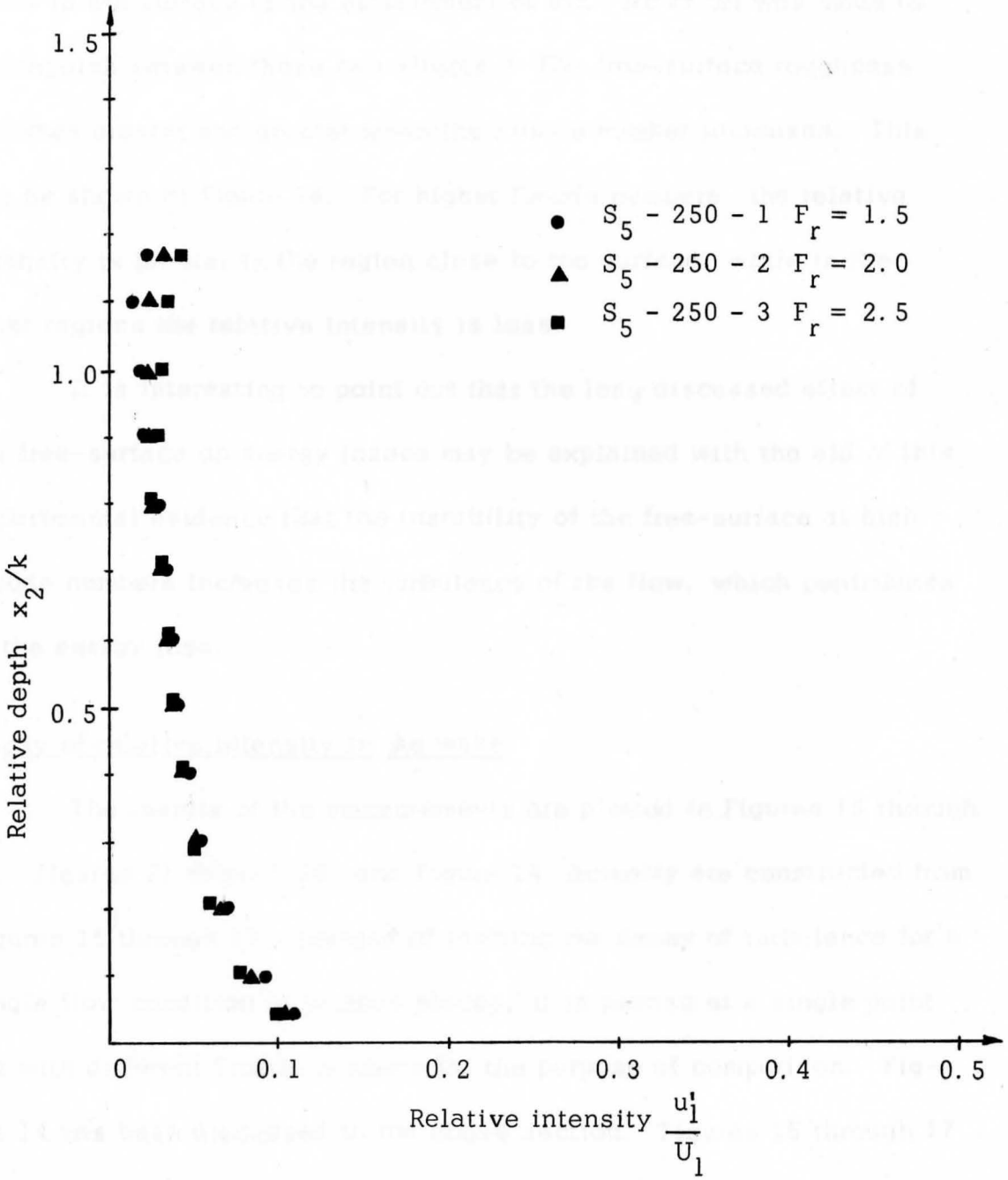

Figure 14. Comparison of the relative intensity for different Froude numbers. (Undisturbed velocity profile.)

(Another possible reason for increase in the apparent intensity close to the surface is the entrainment of air. No effort was made to distinguish between these two effects.) The free-surface roughness becomes greater and greater when the Froude number increases. This can be shown in Figure 14. For higher Froude numbers, the relative intensity is greater in the region close to the surface, while in the other regions the relative intensity is less.

It is interesting to point out that the long discussed effect of the free-surface on energy losses may be explained with the aid of this experimental evidence that the instability of the free-surface at high Froude numbers increases the turbulence of the flow, which contributes to the energy loss.

Decay of relative intensity in the wake

The results of the measurements are plotted in Figures 15 through 26. Figures 21 through 26 and Figure 14, actually are constructed from Figures 15 through 17. Instead of plotting the decay of turbulence for a single flow condition at various places, it is plotted at a single point but with different Froude numbers for the purpose of comparison. Figure 14 has been discussed in the above section. Figures 15 through 17 for the depth of 0.25 feet are quite similar to Figures 18 through 20, and the effect due to the difference of depth (due to the different submergence ratio) is not so evident. However, the effect due to Froude number is clear.

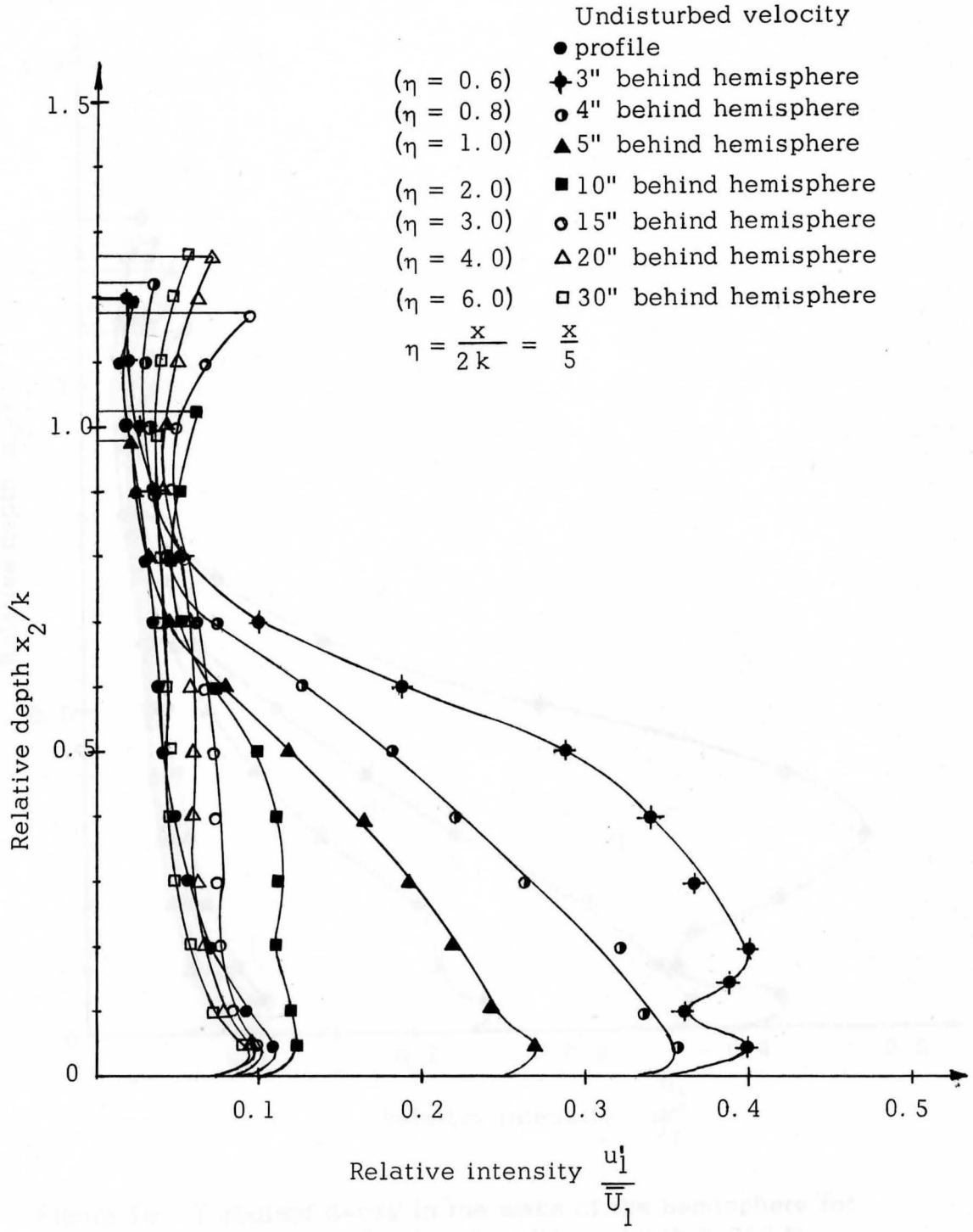

Figure 15. Turbulent decay in the wake of the hemisphere for S5-250-1 . (Undisturbed flow: depth 0.250 ft., Froude No. 1.5)

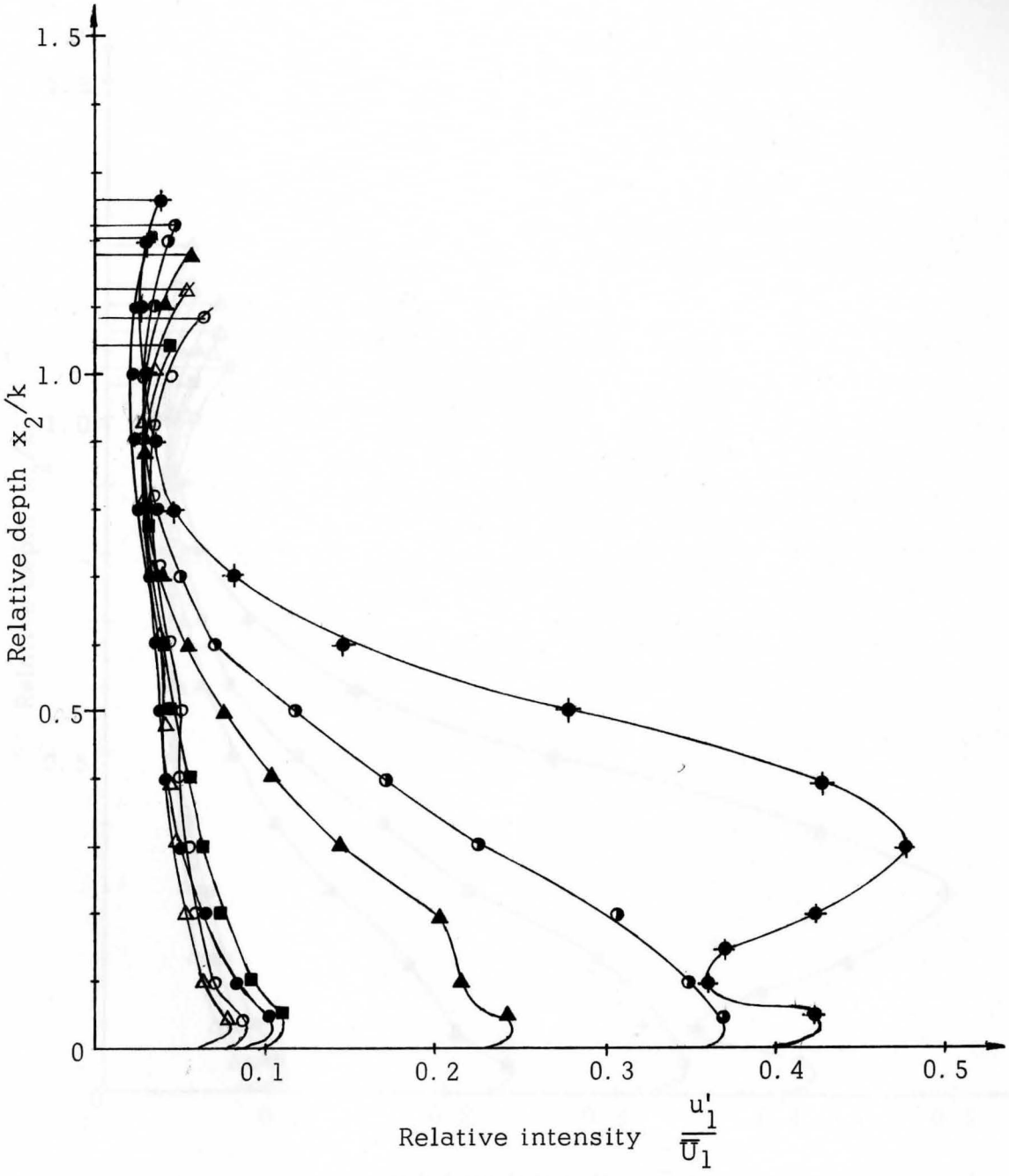

Figure 16. Turbulent decay in the wake of the hemisphere for S5-250-2. (Undisturbed flow: depth 0.250 ft, Froude No. 2.0.)

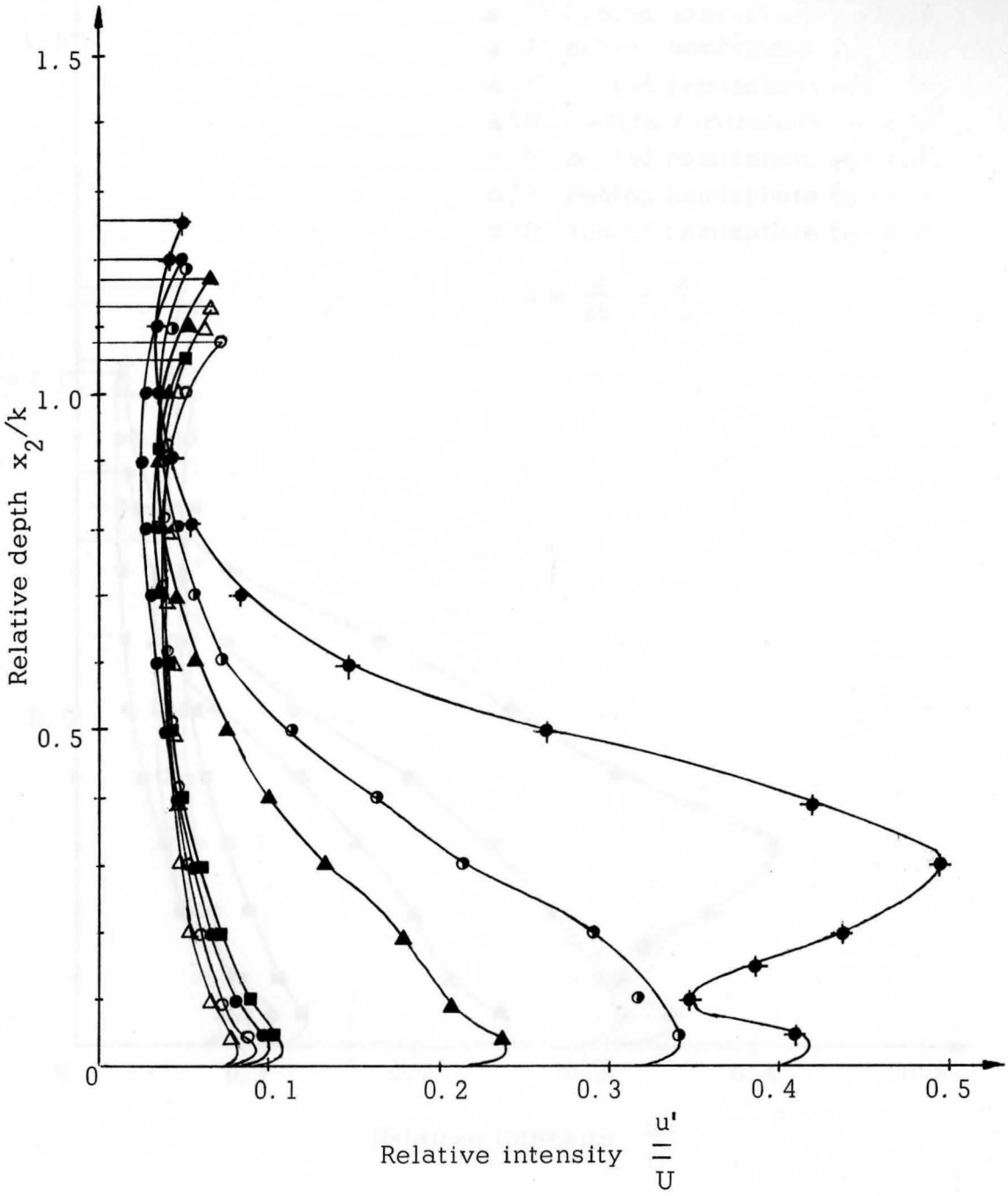

Figure 17. Turbulent decay in the wake of the hemisphere for S5-250-3 . (Undisturbed flow: depth 0.250 ft. Froude No. 2.5.)

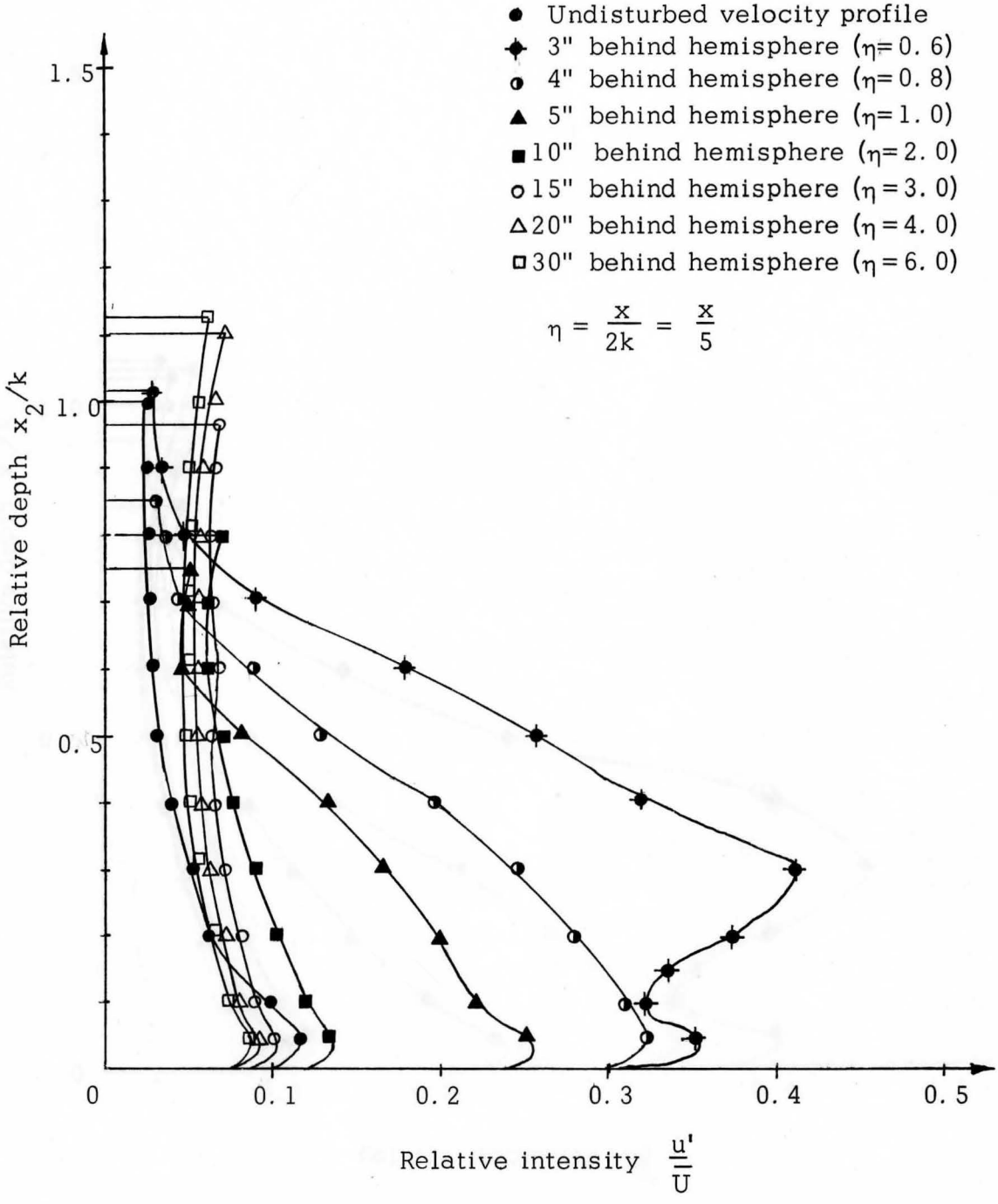

Figure 18. Turbulent decay in the wake of the hemisphere for S5-208-1 . (Undisturbed flow: depth 0. 208 ft. Froude No. 1. 5 .)

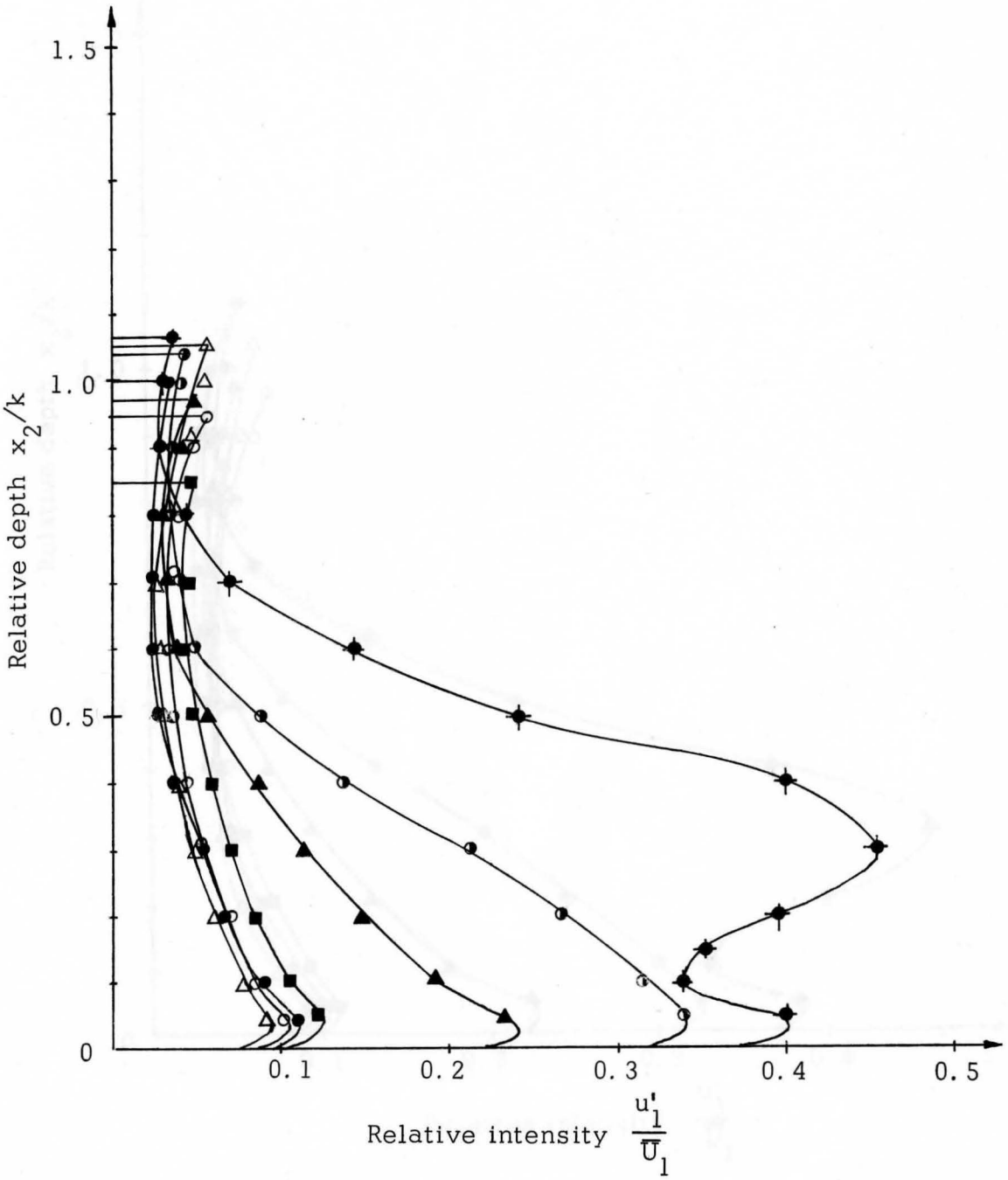

Figure 19. Turbulent decay in the wake of hemisphere for S5-208-2 . (Undisturbed flow: depth 0.208 ft.) (Froude number 2.0.)

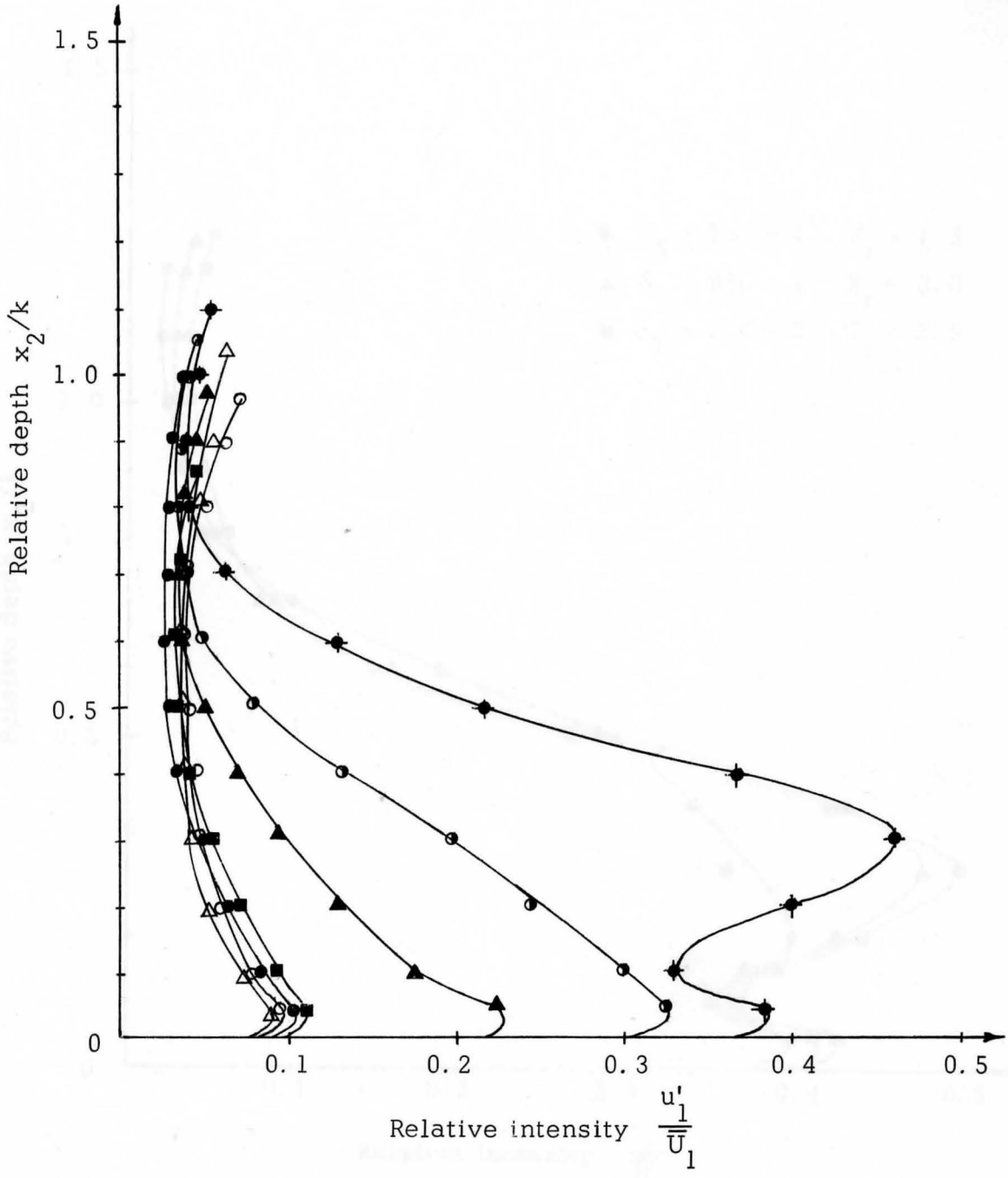

Figure 20. Turbulent decay in the wake of hemisphere for S5-208-3. (Undisturbed flow depth 0.208 ft. Froude number 2.5.)

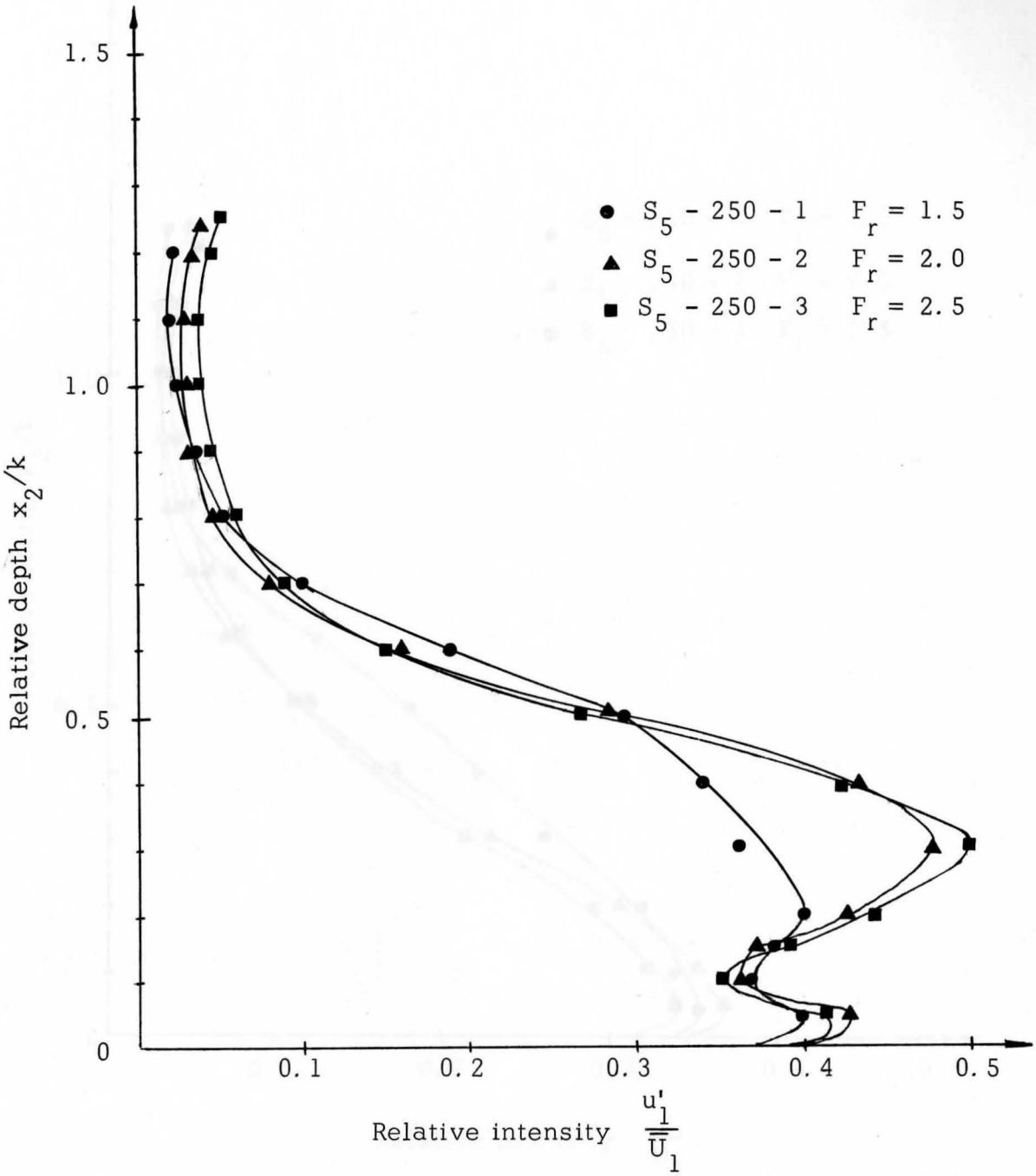

Figure 21. Comparison of the relative intensity for different Froude No. in the wake of hemisphere (3" behind the hemisphere).

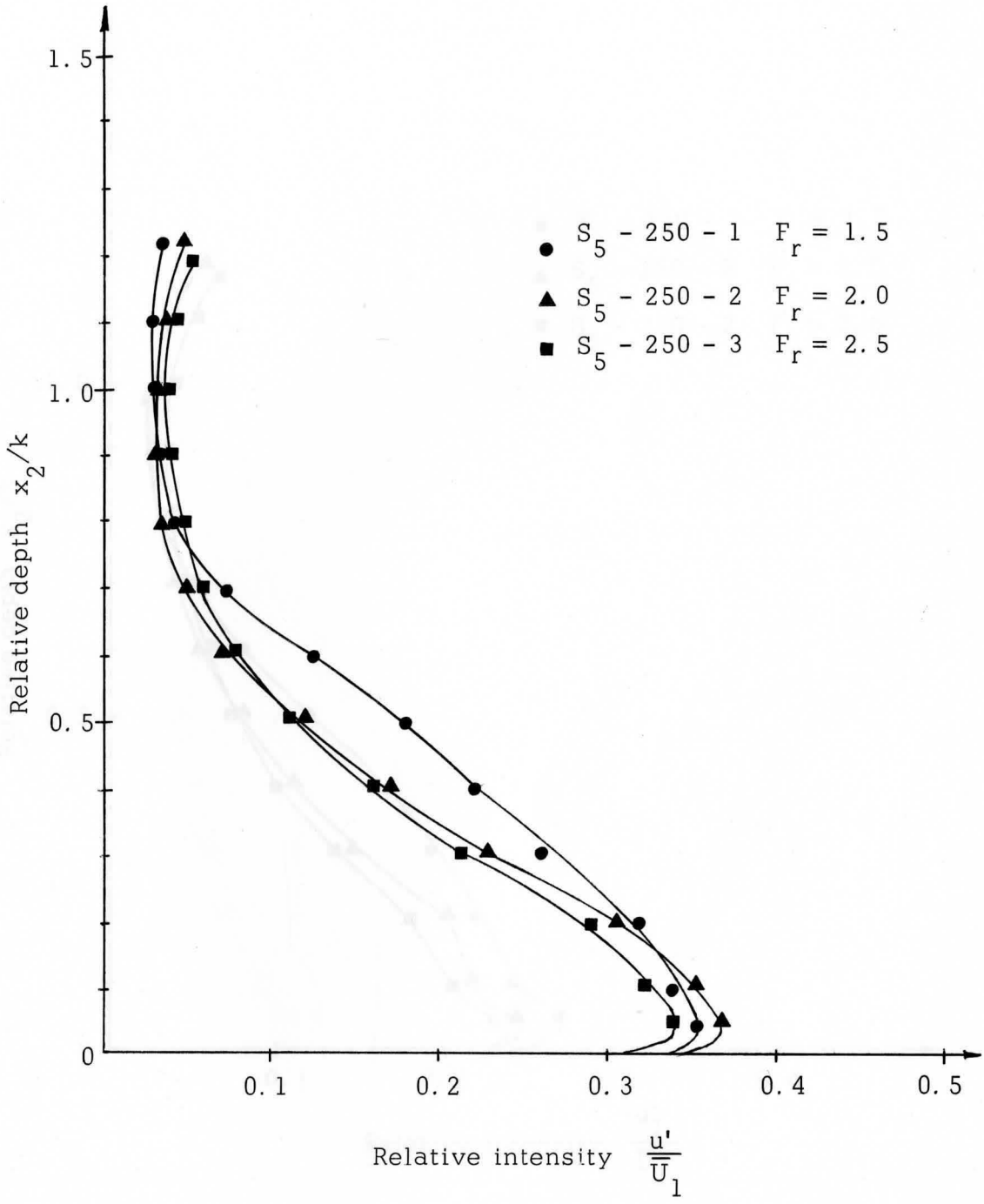

Figure 22. Comparison of the relative intensity for different Froude No. in the wake of hemisphere (4" behind the hemisphere).

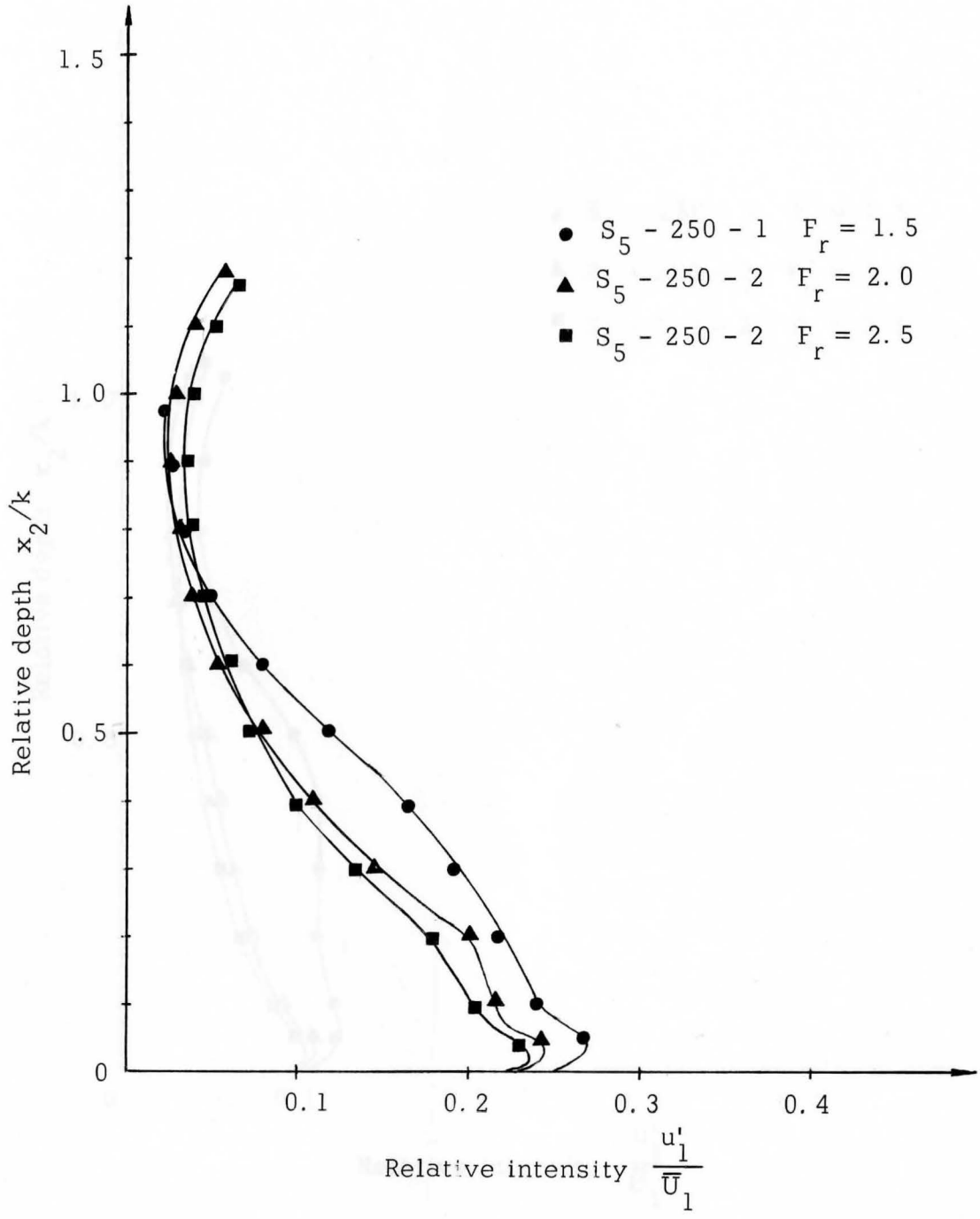

Figure 23. Comparison of the relative intensity for different Froude No. in the wake of hemisphere (5" behind the hemisphere).

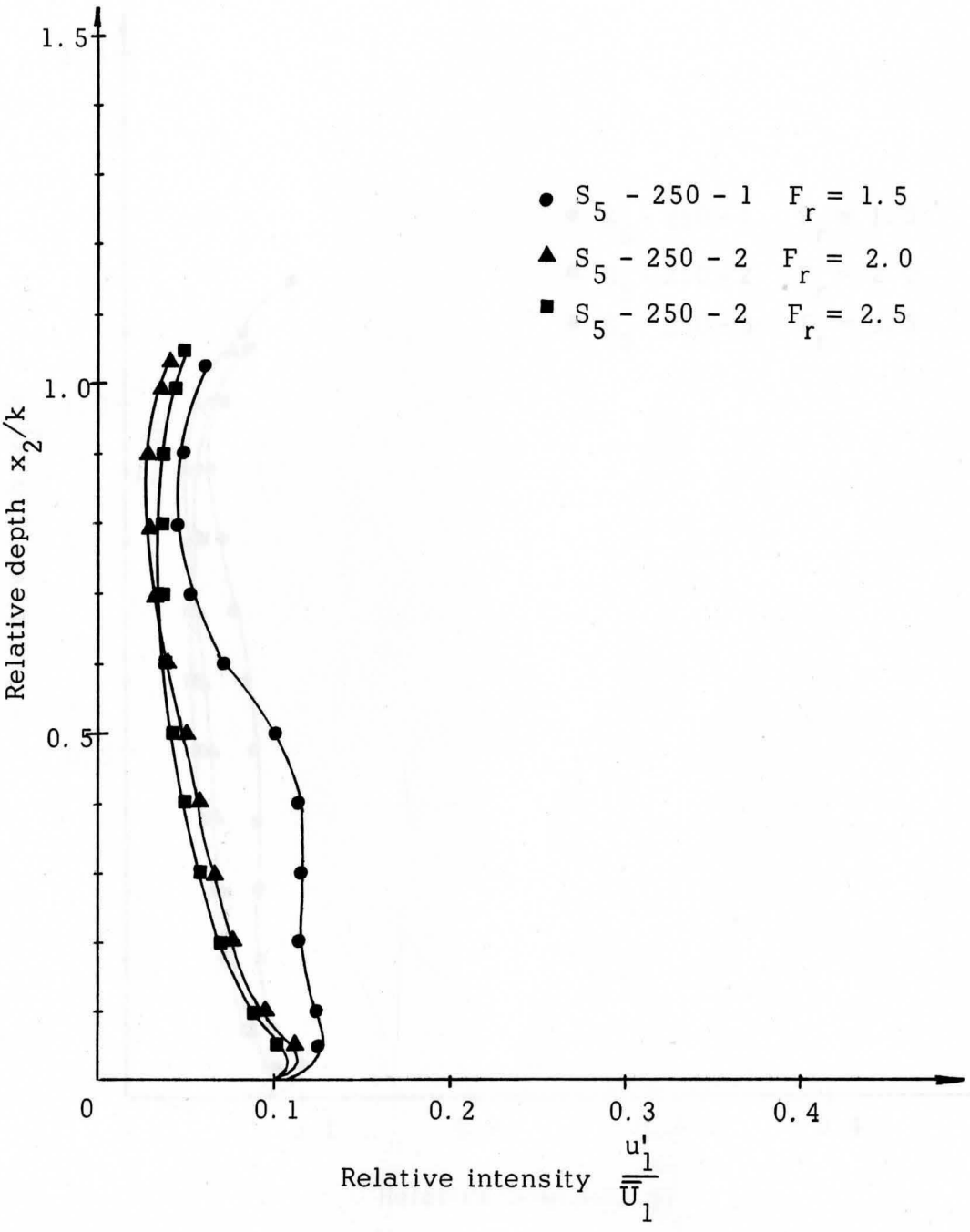

Figure 24. Comparison of the relative intensity for different Froude No. in the wake of hemisphere (10" behind the hemisphere).

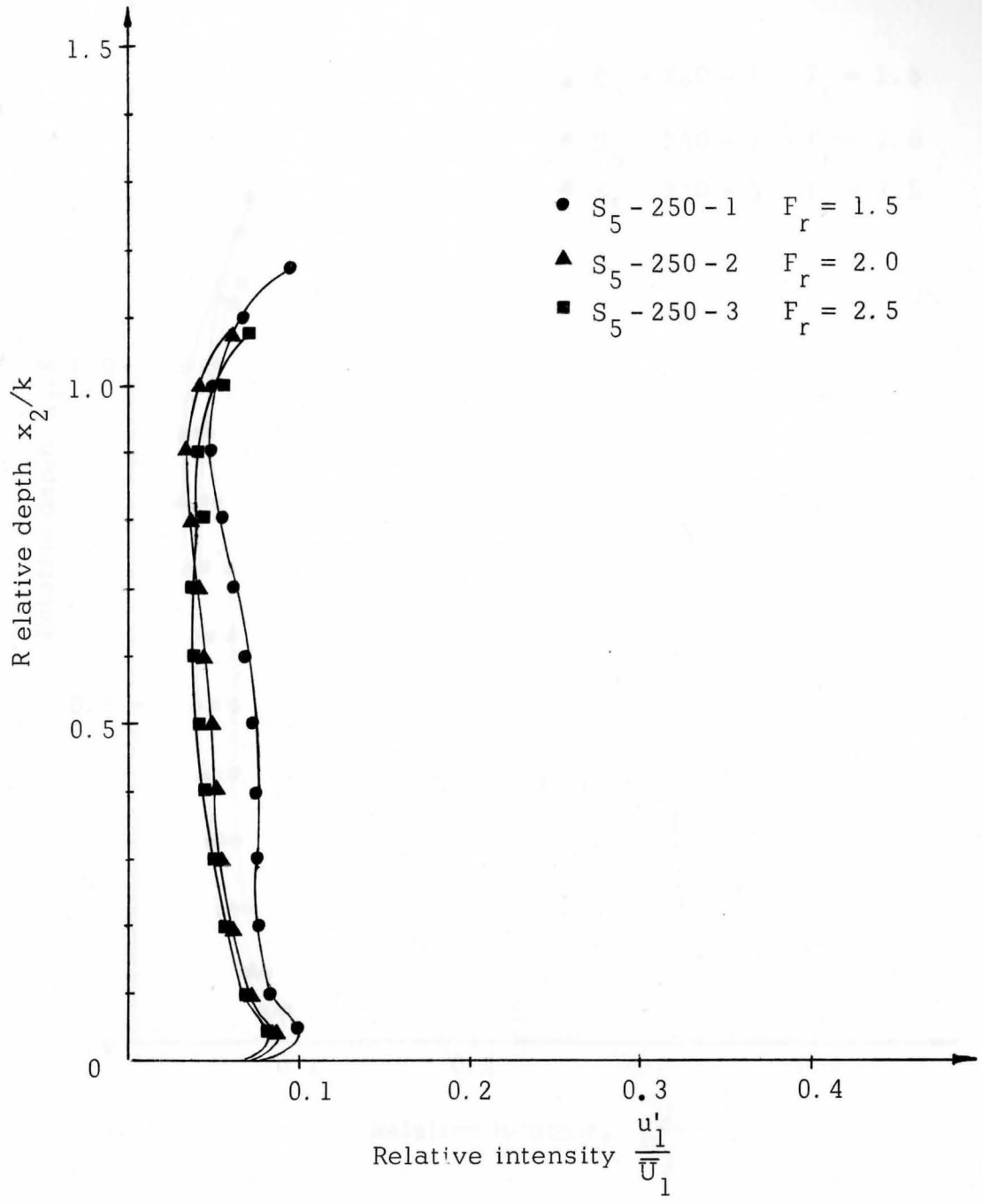

Figure 25. Comparison of the relative intensity for different Froude No. in the wake of hemisphere (15" behind the hemisphere).

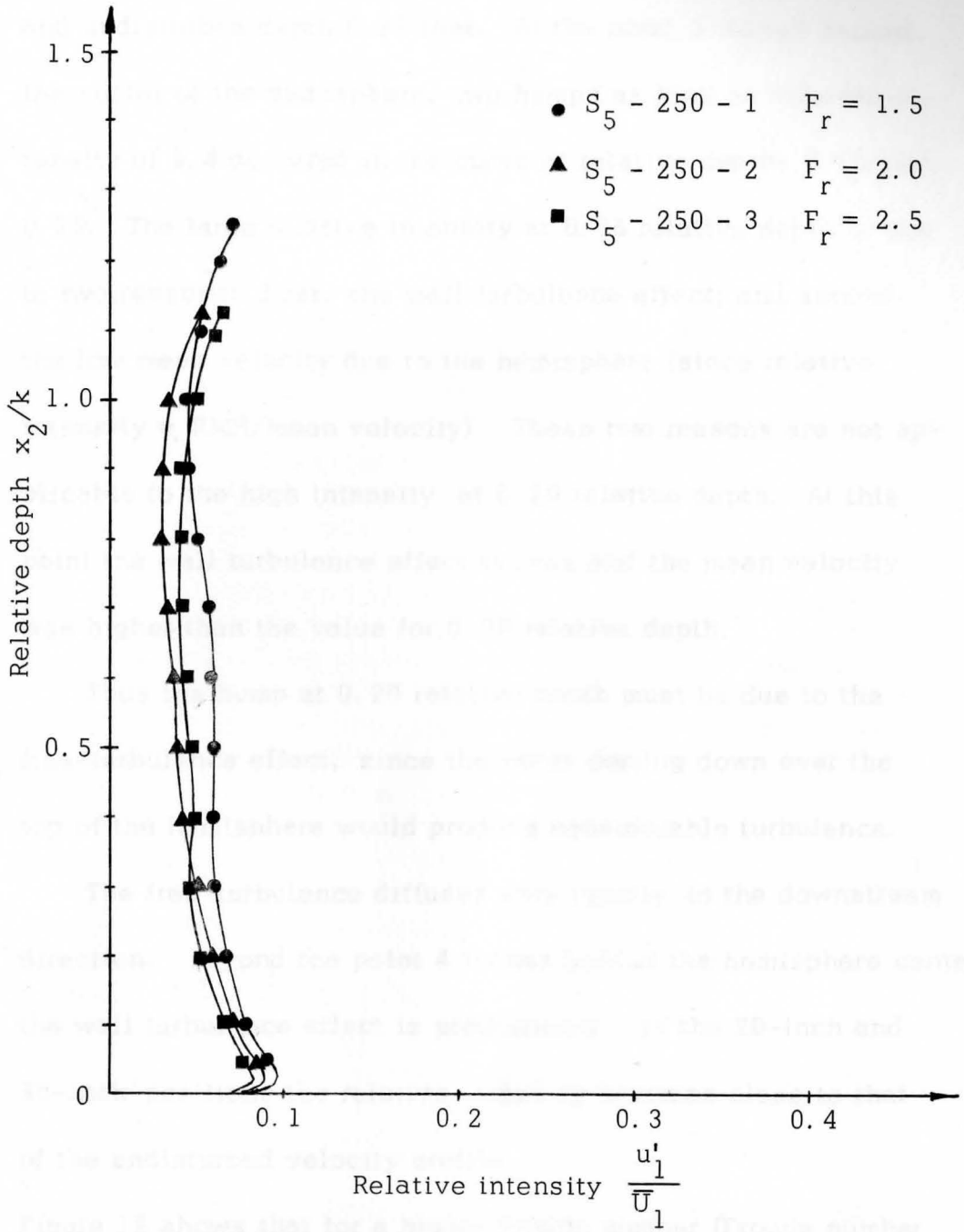

Figure 26. Comparison of the relative intensity for different Froude No. in the wake of hemisphere (20" behind the hemisphere).

Several conclusions can be drawn at this moment:

(a) Figure 15 shows the turbulence decay for Froude number 1.5 and undisturbed depth 0.25 feet. At the point 3 inches behind the center of the hemisphere, two humps as high as relative intensity of 0.4 occurred in the curve at relative depths 0.05 and 0.20. The large relative intensity at 0.05 relative depth is due to two reasons: first, the wall turbulence effect; and second, the low mean velocity due to the hemisphere (since relative intensity = RMS/mean velocity). These two reasons are not applicable to the high intensity at 0.20 relative depth. At this point the wall turbulence effect is less and the mean velocity was higher than the value for 0.05 relative depth.

Thus the hump at 0.20 relative depth must be due to the free-turbulence effect, since the water coming down over the top of the hemisphere would produce considerable turbulence.

The free turbulence diffuses very rapidly in the downstream direction. Beyond the point 4 inches behind the hemisphere center the wall turbulence effect is predominant. In the 20-inch and 30-inch positions the relative intensity becomes close to that of the undisturbed velocity profile.

(b) Figure 16 shows that for a higher Froude number (Froude number 2.0), the free-turbulence effect is so great that the relative intensity reaches a high of 0.48 at the position 3 inches behind the hemisphere center. The free-turbulence effect at this point is

greater than the wall turbulence effect. The turbulence decay was so rapid that at 10 inches behind the hemisphere center the relative intensity was almost the same as that of the undisturbed velocity profile. Figure 17 for a Froude number of 2.5 shows an even greater hump in the position 3 inches behind the hemisphere center. Figures 18, 19, and 20 for the undisturbed flow depth of 0.208 feet, which corresponds to the submergence ratio 1.0, show similarly shaped curves. The same reasoning will apply to explain these results.

(c) Figure 21 shows the relative intensity at 3 inches behind the hemisphere center for 3 different Froude numbers. The higher Froude number shows greater free-turbulence effect both in the second hump (0.3 relative depth) and the region close to the surface. Figure 22 proves that the free-turbulence diffuses so rapidly that the great free-turbulence in the second hump at 0.3 relative depth soon disappears. The wall turbulence still dominates in the wall region.

The surface region still shows that the higher Froude number has the higher free-turbulence effect. Figures 23 through 26 also show that higher Froude number flows decay faster and the relative intensity is greater only in the region close to the surface. This occurs because the higher the Froude number, the greater the turbulent energy that the flow possesses, which enables the wake region

to recover faster to the undisturbed relative intensity. Therefore the turbulence produced by the hemisphere will decay faster at higher Froude number.

A Note on the Temperature of the Water

Since the whole principle of hot-wire anemometry is based on the heat transfer relation between the sensor element and the fluid flow past the sensor, any change in the water temperature will effect the heat transfer relation and change the sensor calibration. Much care was taken in this regard. The water temperature was constantly measured at intervals of about 30 minutes. In the winter it was found that the temperature remained essentially constant during the time needed for one run. In the summer it was found that the variation of the water temperature was about 2 degrees during the day.

CHAPTER V

CONCLUSIONS AND SUGGESTIONS FOR FURTHER RESEARCH

Conclusions

Some conclusions can be made from this experimental study concerning the turbulent decay in the wake of the hemisphere.

(1) In the wake of the hemisphere a periodic phenomena exist which are similar to the Karman vortex street. The autocorrelations become weaker and weaker in the downstream direction. The macro scale of turbulence is decreasing as the point of measurement moves in the downstream direction.

(2) At higher Frounde numbers the relative intensity of the undisturbed velocity profile is higher in the region close to the free-surface. The instability of the free-surface at high Froude numbers increases the turbulence of the flow in the region close to the surface.

(3) In the wake of the hemisphere the relative intensity decreases in the downstream direction except in the region very close to the free-surface.

(4) In the position 3 inches behind the hemisphere center the free-turbulence effect is so strong that the greatest relative intensity is not in the region close to the channel

bed but, rather, a short distance above. Higher Froude numbers have greater free-turbulence effects.

(5) The diffusion of the free turbulence is so rapid that the wall turbulence predominates in the position 4 inches behind the hemisphere center.

(6) The decay of relative intensity is faster for higher Froude number flow.

Suggestions for Further Research

Because of the difficulties in using the cylindrical hot-film or X-array hot-film sensor in water containing impurities a filtration of the water would be necessary for further research. The recommendations can be listed as follows.

(1) Use a recirculating flume and filter the water constantly to remove the impurities in the water such as sediment, hairs, lint, algae, etc., in order that the calibration curve of the sensor may be applicable for longer period.

(2) Use the X-array probe to obtain the turbulent shear in the wake region and use two identical probes to measure the space correlations in the wake and obtain a more complete survey of the characteristics in the wake region.

(3) Use the reflection technique to eliminate the free-surface effect and compare this with the results having the free-surface to determine the effect of the free-surface on the turbulence.

LITERATURE REFERENCES

Batchelor, G. K. 1953. The theory of homogeneous turbulence. Cambridge University Press, Cambridge, Great Britain. 197 p.

Clyde, Calvin G. and H. A. Einstein. 1966. Fluctuating total head in a viscous sublayer. Journal of the Engineering Mechanics Division, Proceedings of the American Society of Civil Engineers 92:EM 2:251-275.

Dryden, H. L. 1943. Review of statistical theory of turbulence. Quarterly, Applied Mathematics: 1:7-42.

Dryden, H. L. 1951. The turbulence problem today. Proceedings of the First Midwestern Conference on Fluid Mechanics. J. W. Edward, Ann Arbor Michigan. pp. 1-20.

Goldstein, S. 1938. Modern developments in fluid dynamics. Volumes I and II, Oxford University Press, London. 702 p.

Goldstein, S. 1951. On the law of decay of homogeneous isotropic turbulence and the theory of the equilibrium and similarity spectra. Proceedings Cambridge Philosophical Society, Cambridge, England.

Heisenberg, W. 1948. On the theory of statistical and isotropic turbulence. Proceedings of the Royal Society of London. Series A. 195:402-406.

Hinze, J. O. 1959. Turbulence. McGraw-Hill, New York. 586 p.

Hubbard, Philip G. 1957. Operating manual for the II HR hot-wire and hot-film anemometers. State University of Iowa Press. Ames, Iowa.

Kolmogoroff, A. N. 1941. The local structure of turbulence in incompressible viscous fluid for very large Reynolds number. U. S. S. R. Academy of Science in English translation. New York. 30:301-305.

Kolmogoroff, A. N. 1941. On degeneration of isotropic turbulence in an incompressible viscous fluid. U. S. S. R. Academy of Science in English translation. New York. 31:538-540.

Kolmogoroff, A. N. 1941. Dissipation of energy in locally isotropic turbulence. U. S. S. R. Academy of Science in English translation. New York. 32:16-18.

Lin, C. C. 1948. Note on the law of decay of isotropic turbulence. Proceedings National Academy of Science. Washington, D. C. 34:540-543.

Lin, C. C. 1961. Statistical theories of turbulence. Pinceton University Press, New Jersey. 60 p.

Pai, S. I. 1957. Viscous flow theory, Volume II Turbulent flow. Van Nostrand, Princeton, New Jersey. 277 p.

Schlichting, H. 1960. Boundary layer theory. McGraw-Hill Book Company, New York. 586 p.

Taylor, G. I. 1935. Statistical theory of turbulence. Part I-IV. Proceedings of the Royal Society of London. Series A. 151:421-478.

Taylor, G. I. 1938. The spectrum of turbulence. Proceedings of the Royal Society of London. Series A 164:476-490.

Townsend, A. A. 1947. Measurements in the turbulent wake of a cylinder. Proceedings of the Royal Society of London. Series A 190:551-561.

Townsend, A. A. 1949. Momentum and energy diffusion in the turbulent wake of a cylinder. Proceedings of the Royal Society of London. Series A. 197:124-140.

Townsend, A. A. 1956. The structure of turbulent shear flow. Cambridge University Press, Cambridge, Great Britain. 315 p.

Von Karman, T. 1938. On the statistical theory of isotropic turbulence. Proceedings of the Royal Society of London. A164: 192-215.

Von Karman, T. 1948. Progress in the statistical theory of turbulence. Journal of Marine Research. New Haven, Connecticut. 7:252-264.

LIST OF SYMBOLS AND DEFINITIONS

$\overline{A}$	Time average of the quantity A .
F_r	Froude number $\left(\frac{V}{\sqrt{g \cdot d}}\right)$ where d = depth of flow.
$f(x)$	Distribution function of the random variable x .
k	Radius of the hemisphere (in this study k is 0. 208 ft) .
L_{x_i}	Macroscale of turbulence based on the velocity correlation along x_i axis .
$R_{ij} = \frac{\overline{u_i u'_j}}{\sqrt{\overline{u_i^2}\ \overline{u'^2_j}}}$	Double-velocity correlation coefficient .
$R_i(\tau) = \frac{\overline{u_i(t)\ u_i(t+\tau)}}{\overline{u_i^2}}$	Autocorrelation coefficient .
$R.I. = \frac{\sqrt{\overline{u_i^2}}}{\overline{U}_i} = \frac{u'_i}{\overline{U}_i}$	Relative intensity .
$\overline{U}_1,\ \overline{U}_2,\ \overline{U}_3,$	Mean velocity along $x_1,\ x_2,\ x_3,$ (x, y, z) axis .
$u_1,\ u_2,\ u_3,$	Turbulent fluctuation along $x_1,\ x_2,\ x_3$ (x, y, z) axis .
$V_i = \overline{U}_i + u_i$	Velocity in the x_i direction (i = 1, 2, 3) .
$u' = \sqrt{\overline{u^2}}$	Root mean square value of the turbulent fluctuation .
x_2	Depth of the flow .

x_2/k	Relative depth .
τ	Time delay in millisecond .
$\tau_{ij} = -\rho \overline{u_i u_j}$	Reynold's stress .
σ_{ij}	Stress tensor due to pressure and viscous forces.
λ_f	Microscale of turbulence .
$\eta = \frac{x_1}{2K}$	Dimensionless parameter, x_1 is the distance between the center of hemisphere and the point of observation in the wake, 2K is the diameter of the hemisphere .
μ_1	Mean (first moment about the origin) .
μ_2	Variance (second moment about the mean) .